Published in final edited form as:

Cell Rep. 2024 March 26; 43(3): 113886. doi:10.1016/j.celrep.2024.113886.

Non-canonical isoforms of the mRNA polyadenylation factor WDR33 regulate STING-mediated immune responses

Lizhi Liu[1,2], **James L. Manley**[1,3,*]

[1]Department of Biological Sciences, Columbia University, New York, NY 10027, USA

[2]Present address: RNA Division, New England Biolabs, Inc, Beverly, MA 01915, USA

[3]Lead contact

SUMMARY

The human *WDR33* gene encodes three major isoforms. The canonical isoform WDR33v1 (V1) is a well-characterized nuclear mRNA polyadenylation factor, while the other two, WDR33v2 (V2) and WDR33v3 (V3), have not been studied. Here, we report that V2 and V3 are generated by alternative polyadenylation, and neither protein contains all seven WD (tryptophan-aspartic acid) repeats that characterize V1. Surprisingly, V2 and V3 are not polyadenylation factors but localize to the endoplasmic reticulum and interact with stimulator of interferon genes (STING), the immune factor that induces the cellular response to cytosolic double-stranded DNA. V2 suppresses interferon-β induction by preventing STING disulfide oligomerization but promotes autophagy, likely by recruiting WIPI2 isoforms. V3, on the other hand, functions to ncrease STING protein levels. Our study has not only provided mechanistic insights into STING regulation but also revealed that protein isoforms can be functionally completely unrelated, indicating that alternative mRNA processing is a more powerful mechanism than previously appreciated.

Graphical Abstract

*Correspondence: jlm2@columbia.edu.

AUTHOR CONTRIBUTIONS

L.L. and J.L.M. conceived the study. L.L. performed experiments and analyzed data. L.L. wrote the manuscript. J.L.M. and L.L. edited the manuscript.

SUPPLEMENTAL INFORMATION

Supplemental information can be found online at https://doi.org/10.1016/j.celrep.2024.113886.

DECLARATION OF INTERESTS

The authors declare no competing interests.

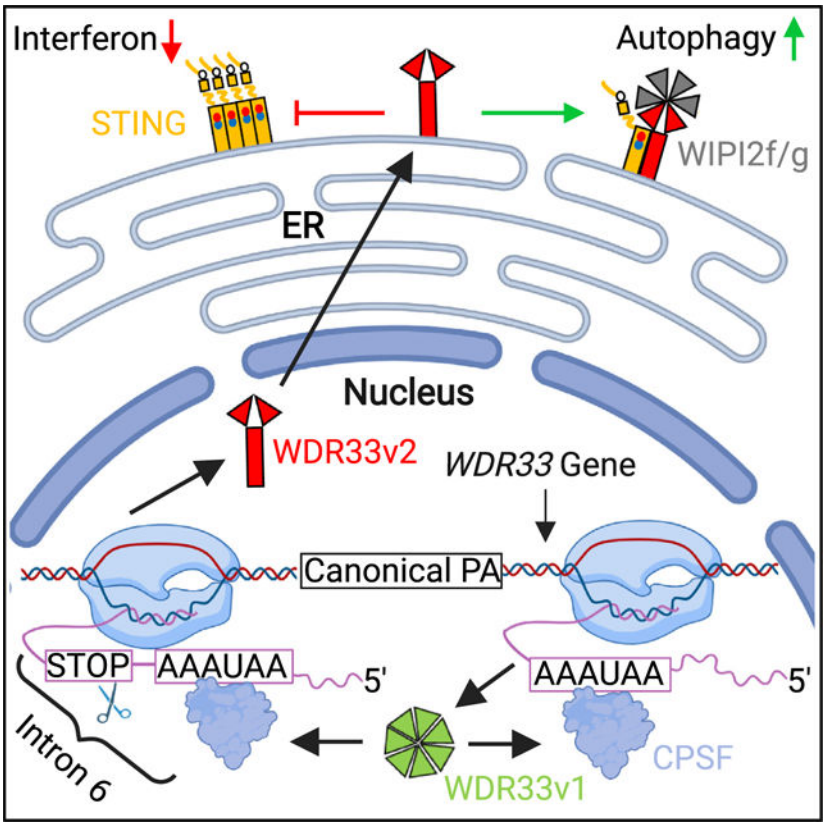

In brief

Liu and Manley report that two noncanonical isoforms of the mRNA poly(A) factor WDR33, arising from alternative polyadenylation, are not themselves poly(A) factors but are regulators of the immune factor STING. This study provides a striking example showing that alternative mRNA processing can produce proteins that are functionally completely unrelated.

INTRODUCTION

The final step of mRNA biogenesis involves the endonucleolytic cleavage of the nascent mRNA at its 3′ end and the synthesis of a poly(A) tail, two coupled reactions known as cleavage and polyadenylation (CPA). The cleavage and polyadenylation specificity factor (CPSF) is a core component of the mammalian CPA machinery. It consists of six subunits and is indispensable for CPA.[1,2] Among these, two subunits, CPSF30 and WDR33, confer CPA specificity by recognizing the A[A/U]UAAA polyadenylation signal (PAS), a highly conserved RNA element within the polyadenylation site.[3–6]

The human *WDR33* genes encode three major isoforms.[7] The canonical isoform, WDR33v1 (V1), a WD (tryptophan-aspartic acid) repeat protein containing seven N-terminal repeats that form a β-propeller, recognizes the PAS.[5,6] Two non-canonical isoforms, WDR33v2 (V2) and WDR33v3 (V3), contain only the first two or three WD repeats, respectively. Interestingly, the rat V2 homolog was initially discovered over 20 years ago in a nuclear envelope proteomic study and named NET14 (Nuclear Envelope Transmembrane 14).[8]

However, its localization has not been verified and its function is unknown. V3 has not been studied.

Approximately 70% of mammalian genes harbor multiple polyadenylation sites, commonly within 3′ untranslated regions (3′ UTRs) or introns.[9,10] Usage of different polyadenylation sites is known as alternative polyadenylation (APA).[11,12] When APA occurs within the 3′ UTR, it alters an mRNA's 3′ UTR length, affecting its stability and/or translation efficiency. Intronic APA (IPA), in which CPA occurs within intronic sequences, can retain a portion of the intron, thereby altering the mRNA coding sequence (CDS). Thus, similar to alternative splicing (AS), IPA can generate distinct protein isoforms and contribute to proteome diversity.

STING (stimulator of interferon genes) is an immune factor that induces a variety of immune responses. It localizes to the endoplasmic reticulum (ER) and plays a central role in the cGAS-STING pathway that is activated in the presence of cytosolic doublestranded DNA (dsDNA), which often results from DNA virus infection or intracellular damage.[13,14] cGAS (cyclic GMP-AMP synthase) recognizes cytosolic dsDNA and produces the second messenger 2′3′-cyclic GMP-AMP (cGAMP), which binds to and activates STING.[15,16] Activated STING oligomerizes by forming disulfide bonds between monomers at Cys148[17] and is then exported out of the ER.[18] During transport, STING is phosphorylated by TBK1 at Ser366,[19] which is required for activation of the transcription factor interferon regulatory factor 3 (IRF3).[20] STING also activates nuclear factor κB (NF-κB) independent of ER exit or TBK1, but the mechanism is unclear.[21] IRF3 and NF-κB activation ultimately leads to induction of immune cytokines, such as interferons and interleukins. It has been proposed that STING oligomerization is required for Ser366 phosphorylation, because, based on the structure of STING-TBK1, the kinase domain of TBK1 can only reach Ser366 of the STING adjacent to the one to which TBK1 binds directly.[22] However, whether or not phosphorylated STING monomers exist has not been determined experimentally. Currently, no regulators of STING disulfide oligomerization have been identified.

In addition to immune cytokine induction, STING can also activate autophagy, a lysosome-dependent degradation mechanism, as a means to eliminate invading pathogens.[14] Production of autophagosomes, which are vesicles that engulf cytoplasmic components and deliver them to the lysosome for degradation, is a multi-step process that culminates in the conversion of the LC3 protein from the inactive form (LC3-I) to the activated phosphatidylethanolamine-conjugated form (LC3-II).[23] Autophagy induction by STING is independent of Ser366 phosphorylation as well as many early autophagy factors, such as ULK1 and the Beclin complex.[24] It does, however, require the WD protein WIPI2, which directly interacts with STING and other downstream autophagy factors.[24–26] Regulation of STING-induced autophagy is not well understood.

In this study, we characterized V2 and V3 and investigated their regulation and functions. Our interest in these two WDR33 isoforms arose from a previous RNA-sequencing (RNA-seq) study from our lab,[27] in which we identified an AS event that appeared to generate V2 as human embryonic stem cells (hESCs) differentiated into trophoblasts and neural progenitor cells. Subsequent analyses, however, revealed that V2, and V3, do not arise from

AS, and their expression levels do not change during hESC differentiation. Nevertheless, we continued analysis of V2 and V3 and found that they are created by IPA-related mRNA processing. Remarkably, we also found that V2 and V3 are not polyadenylation factors localized to the nucleus like V1 but instead are immune factors localized to the ER and function in the regulation of STING-mediated immune responses. Our study not only provides unexpected insights into the cGAS-STING pathway but also, more broadly, serves as a striking example of how protein isoforms produced by alternative mRNA processing can have completely unrelated functions.

RESULTS

V2 and V3 mRNAs are generated by APA

The human *WDR33* gene encodes three major mRNA isoforms. According to RefSeq,[7] complete removal of all 21 introns generates the canonical full-length mRNA, V1 (initially called WDC146[28]). Both V2 and V3 mRNAs terminate in intron 7. Intron 6 is retained in V2, and a portion of intron 7 is removed in V3 using an upstream alternative 3′ splice site (SS) (Figure 1A). V2 and V3 CDSs end within introns 6 and 7, respectively. By analyzing published RNA-seq datasets,[29,30] we found that both A549 and HeLa cells have virtually identical WDR33 isoform expression profiles (Figure 1B). V1 is the most abundant, followed by V2 (~50% of V1), while expression of V3 is very low (~5% of V1). We detected expression of all three isoform mRNAs by RTPCR in HeLa, 293T, U2OS, U87, Raji, H9 hESCs, and differentiating embryoid bodies derived from H9 cells, indicating that WDR33 isoform expression is not cell-type specific (Figure 1C). This is consistent with findings by Ito et al. with various mouse tissues.[28] While expression of V1 was significantly decreased during hESC differentiation, V2 and V3 levels were largely unchanged (Figure S1A).

We next wished to gain insight into how V2 and V3 are formed. We therefore examined human *WDR33* genomic regions corresponding to V2 and V3 mRNA 3′ ends and identified multiple potential PASs (Figure S1B). V2 PASs are scattered in introns 6 and 7, and in exon 7; there are five PASs downstream of the stop codon (PAS1–5), and there is one PAS within the CDS (PAS0), 12 nt upstream of the stop codon. For V3 there are six PASs, all within intron 7 and downstream of the stop codon. Based on rapid amplification of cDNA 3′ ends (3′ RACE), PAS0, PAS3, and PAS5 for V2, and PAS1, PAS3/4, and PAS5 for V3 are functional (Figures 1D and S1C). V2 PAS usage is especially noteworthy. PAS0 usage (intron 6) generates a 3′ UTR-less mRNA with an unaltered CDS, as the associated cleavage site is within the stop codon (Figure 1E). PAS3 usage (exon 7) is an unusual exonic APA event and results in intron 6 retention. Since PAS3 is only 16 nt downstream of the intron 6 3′ SS, assembly of the CPA machinery there likely interferes with 3′ SS recognition (Figure 1F). PAS5 usage (intron 7) also causes intron 6 retention, but it is not clear how this is achieved. Thus, V2 mRNA can terminate not only in intron 7 but also in intron 6 and exon 7. V3 PAS usage, in contrast, appears unexceptional. These results suggest that V2 and V3 mRNAs are generated by IPA as well as exonic APA.

V2 and V3 proteins interact with and stabilize each other

V1 is a large protein with seven N-terminal WD repeats. V2 and V3 proteins would be much shorter, with only the first two or three WD repeats, respectively (Figure 2A). The C termini of V2 and V3, which result from the retention of a portion of introns 6 and 7, respectively, are distinct and specific to each protein. While we were unsuccessful in obtaining antibodies (commercial or custom) that could detect V2/V3 proteins, we did detect association of V2 mRNA with ribosomes by analyzing a published ribosome profiling dataset of 293 cells,[31] which indicated that V2 mRNAs are actively translated (Figure S2A). Also, as mentioned in the introduction, rat V2 was detected in a previous proteomics analysis.[8] We did not detect V3 mRNAs, likely due to its much lower expression (see above).

It has been shown that artificially truncated WD proteins with an insufficient number of repeats can interact to form a complete β-propeller *in vitro*.[32] In light of this, we performed co-immunoprecipitation (coIP) using an FLAG antibody with extracts of 293T cells expressing co-transfected 33FLAG-V2 and HA-V3 (see STAR Methods and Figure S2B for mRNA levels of exogenous V2 and V3). By western blot (WB), we detected interaction between V2 and V3 (Figure 2B). Notably, when co-expressed, V2 and V3 protein levels increased significantly, by ~8-fold and ~1.5-fold, respectively (Figure 2C). No changes in mRNA levels were observed (Figure S2C). However, when we inhibited proteosome-mediated protein degradation by MG132 in V2-/V3transfected cells, V2 and V3 protein levels remained unchanged when co-expressed (Figure 2D). Thus, rather than increasing each other's production, V2 and V3 reduce degradation, signifying a stabilization effect. While it is unclear if V2 and V3 together form a complete β-propeller, our findings nevertheless suggest that WD proteins with insufficient numbers of repeats can interact with and stabilize each other *in vivo*. We term this phenomenon WD repeat complementation (WDRC).

V2 and V3 are not polyadenylation factors

We next investigated whether V2 and V3 are parts of the CPA machinery by examining their interactions with other CPSF subunits. By coIP using an FLAG antibody, we detected interaction of 3× FLAG-V1 with all other CPSF subunits, as expected (Figure 2E). However, interactions with these proteins were not observed with 3×FLAG-V2/V3, expressed individually or together (Figures 2E and S2D). These results are consistent with the finding that rat V2 is a transmembrane protein.[8] Indeed, V2's C terminus (118 amino acids [aa]) is highly hydrophobic and is predicted (~100% confidence) by both TMHMM2 and TMPred to contain at least one transmembrane domain (TMD)[33,34] (Figures S2E and S2F). No TMD was predicted when the V2 C-terminal sequence was removed (FigureS2G). V3's C terminus (16 aa) is likely too short to contain a functional domain.

To extend the above findings, we examined, using immunofluorescence, the subcellular localization of the 33FLAG-tagged WDR33 isoforms. As expected, V1 localized exclusively to the nucleus (Figure 2F). Even though discovered as an NET protein, V2 appeared to localize to the cytoplasm, although signals were strongest just outside of the nucleus (Figure 2F). Notably, NET proteins, but not ER proteins, interact with the nuclear lamina and are resistant to Triton pre-extraction before immunofluorescence fixation.[8] As expected,

the authentic NET protein emerin was resistant to Triton, while V2, like the ER marker calnexin, was sensitive to Triton (Figure S2H). V2 is thus likely an ER protein (ER localization is in fact confirmed below; see Figure 4). V3 displayed strong cytoplasmic signals similarly to V2 and weak nuclear signals (Figure 2F). Based on these findings, we conclude that V2 and V3 are not polyadenylation factors and expect their function(s) to be completely unrelated to that of V1.

V2 and V3 are immune factors regulated by the NF-κB pathway

We next set out to determine the functions of V2 and V3. A previous genome-wide RNAi screen found that WDR33, the function of which was unknown at the time, facilitates influenza A virus (IAV) infection when knocked down.[35] Additionally, IAV infection was found to downregulate V2, but not V1 or V3, expression.[36] These two studies suggest that *WDR33* gene product(s) might be involved in antiviral immune responses. To test this possibility, we first treated HeLa cells with poly(I:C), a synthetic doublestranded RNA (dsRNA) that triggers an immune response associated with RNA virus infection.[37] By RT-qPCR, we confirmed induction of the immune cytokines interferon-β (IFNB1) and interleukin-6 (IL-6) (Figure S3A). Analysis of total WDR33 mRNA levels suggested a slight increase, although the difference was not significant (Figure 3A). However, while V1 levels were not significantly changed, both V2 and V3 levels were markedly increased by ~3-fold (Figure 3A).

To extend these results, we next examined the dsDNA immune response using cGAMP, an endogenous second messenger produced in response to cytosolic dsDNA.[16] For this analysis, we used a derivative of BJ-5ta (BJ) immortalized human fibroblasts that, as described further below, are cGAS $^{-/-}$.[38,39] This was because many commonly used cell lines, including HeLa, fail to induce endogenous immune cytokines upon cGAMP stimulation.[40] We confirmed induction of IFNB1 and IL-6 in these cells following cGAMP treatment (Figure S3B). While total WDR33 mRNA levels were reduced slightly, no change was detected for V1 (Figure 3B). Interestingly, however, V2 and V3 mRNA levels were significantly reduced, by ~50% (Figure 3B). It is notable that V2 and V3 mRNAs exhibited different responses to poly(I:C) and cGAMP. This is not surprising, however, as mRNA expression of immune genes is known to vary significantly depending on the stimulus.[41]

We also performed transcript-level differential expression analyses on a published RNA-seq dataset of SARS-CoV-2-infected cells[30] (Figure 3C and Table S1). We detected a significant upregulation (~2.7-fold) of V2 in ACE2-transfected A549 cells (wild-type [WT] A549 cells do not express ACE2, a cell-surface receptor used by SARS-CoV-2 to infect the host[42]). An increase (~3.3-fold) in V3 was also detected, although the difference was not judged to be significant. V1 expression increased, but only very modestly (~22%). We could not obtain DNA virus infection RNA-seq datasets from cell lines with a functional cGAS-STING pathway. Together, these results imply that V2 and V3, but not V1, may function as immune factors.

We next investigated which immune pathway(s) might regulate V2 and V3 expression. Neither IFNB nor IRF3 are involved, as direct IFNB treatment did not alter V2/V3 expression (Figure S3C), and IRF3 knockdown (KD) did not suppress poly(I:C)-induced

V2/V3 upregulation (Figure S3D). However, when we inhibited the NF-κB pathway with the drug BMS-345541, V2/V3 upregulation following poly(I:C) treatment was no longer detected (Figures 3D and S3E). NF-κB inhibition also prevented cGAMP-induced V2/V3 downregulation in cGAS$^{-/-}$ BJ cells (Figures 3E and S3F). Expression of all three WDR33 isoforms was reduced by ~50%– 70% after BMS-345541 treatment regardless of stimulation or cell line (Figures 3D and 3E), likely reflecting a non-canonical function of the IκB kinase (BMS-345541's target[43]), which is to regulate stability of certain mRNAs.[44] Thus, expression of V2 and V3 is regulated by the NF-κB pathway under both dsRNA and dsDNA immune responses, even though their expression changed in opposite directions.

V2 suppresses cGAMP-induced IFNB1 expression

We next used transient expression assays to investigate V2/V3 function. First, we examined the possible effects of V2 or V3 exogenous expression on poly(I:C)-induced IFNB1 and IL-6 activation in HeLa cells, but no significant effects were observed (Figures S3G and S3H). We next investigated whether V2 and/ or V3 might function in cGAMP-induced immune responses. For this, we used the cGAS$^{-/-}$ BJ cells mentioned above because WT BJ cells with functional cGAS may induce an unwanted immune response by recognizing the transfected plasmid. Importantly, we found that V2-transfected but not V3-transfected cells exhibited significantly lower IFNB1 mRNA levels following cGAMP treatment (Figures S3I and 4A). No change in IL-6 mRNA levels was detected in either V2-or V3-transfected cells (Figure S3J). We note that the observed reduc-tion of IFNB1 mRNA appeared modest (~25%). However, the transfection efficiency in these experiments was also very low (~20%) (Figure S3K), as cGAS$^{-/-}$ BJ cells are difficult to transfect.[39] Thus, the reduction in IFNB1 mRNA per cell by V2 was in fact much greater than 25%. Given that cGAMP functions as an STING ligand,[16] these data suggest that V2 specifically suppresses STING-mediated IFNB1 induction. Furthermore, these data also indicate that high exogenous V3 expression (see Figure S2B) did not alter IFNB1 or IL-6 levels, confirming the specificity of our transient expression approach.

V2 and V3 co-localize and interact with STING

Interestingly, STING was also originally identified as an NET protein (NET23) in the same study that identified V2 (NET14).[8] However, STING was later shown to localize predominately to the ER,[45] as our data above suggest is the case for V2 and V3. We therefore examined possible co-localization of V2/V3 with STING, by co-immunofluorescence of 33FLAG-V1, -V2, or -V3 and STING-HA expressed in 293T cells in the presence or absence of cGAMP (293T cells do not express STING[20]). Strikingly, we detected strong co-localization of both V2 and V3 with STING without cGAMP, confirming that they indeed localize together to the ER (Figures 4B and S4A). We also observed limited V2/V3 (but not STING) cytoplasmic staining outside the ER, indicating that V2 and V3 can localize to additional subcellular regions. We did not identify areas that contained STING but no V2 and V3 signals. Upon cGAMP stimulation, STING oligomerizes and is exported out of the ER.[17,18,46] We confirmed this localization in our cGAMP-treated transfected cells, and, strikingly, observed essentially complete co-trafficking of both V2 and V3 with STING (Figures 4B and S4A). As expected, V1 remained in the nucleus and was physically separate from STING regardless of cGAMP treatment (Figure S4A). While we

always observed co-trafficking of V2 with STING, V3 remained in the cytoplasm following cGAMP treatment in ~20% of cells (Figure S4B).

Since V2 contains a predicted C-terminal TMD, we wondered whether a V2 TMD deletion mutant (V2-dTM, aa 1–208) co-localizes and associates with STING. In the absence of cGAMP, 33 FLAG-V2-dTM localized to both the nucleus and cytoplasm but not the ER, as no V2-dTM/STING overlapping areas were observed (Figure 4C). Following cGAMP treatment, despite formation and trafficking of STING aggregates, V2-dTM did not change its localization and remained unassociated with STING (Figure 4C). Thus, the V2 C terminus indeed contains a TMD that is important not only for V2 ER localization but also for its association with STING, indicating that V2-dTM is a loss-of-function (LOF) mutant. We note that STING-HA localization was exactly as observed with endogenous STING,[24] strongly supporting the validity of our transfection-based approach.

We next examined the possible physical association of these proteins. For this, we performed coIP, using an FLAG antibody for immunoprecipitation with extracts of 293T cells expressing 33FLAG-V1/V2/V3 and STING-HA and an HA antibody for WB to detect STING-HA. Consistent with the co-localization results, we detected interaction between STING and V2 and V3 but not between STING and V1 (Figure S4C). These interactions persisted following cGAMP stimulation (Figure 4D), consistent with co-trafficking of STING with V2 and V3. Following cGAMP treatment, STING is phosphorylated at Ser366,[19] and interestingly no interaction was detected between V2 or V3 and phosphorylated STING (p-STING) by WB using a Ser366 p-STING antibody (Figure 4D). Taken together, these results confirm that V2 and V3, but not V1, are part of the cGAS-STING innate immune pathway.

V2 decreases STING disulfide bond-mediated oligomer accumulation, and both V2 and V3 increase p-STING monomer accumulation

STING oligomerization by disulfide bond formation is required for IFNB1 induction.[17] It is thus possible that V2 suppressed cGAMPinduced IFNB1 expression by preventing STING disulfide oligomerization. To investigate this, we first transiently co-expressed STING-HA with 33FLAG-V2/V3 or empty vector (EV) in 293T cells and examined STING disulfide oligomerization by non-reducing denaturing WB (Figures 5A and S5A). In the absence of cGAMP, V2-transfected cells exhibited increased levels of STING monomers but decreased levels of disulfide dimers (apparent molecular weight [MW] ~75 kDa) compared to the EV control cells, and following cGAMP treatment fewer STING disulfide hexamers (apparent MW ~220kDa) were also detected in the V2-transfected cells. Thus, V2 decreases STING disulfide oligomer accumulation independent of STING activation. V3-transfected cells, however, exhibited increased levels of all STING species (Figure S5B), suggesting that V3 increased overall STING levels. Additionally, levels of 33FLAG-V2 or -V3 were equivalent with or without cGAMP, indicating that there was no cGAMP-dependent regulation of V2/V3 protein levels (Figure S5C).

Since STING Ser366 phosphorylation is required for IFNB1 induction,[20] we also used a Ser366 p-STING antibody to examine p-STING disulfide oligomers. Consistent with the decrease in STING hexamer levels, decreased p-hexamer levels were also detected

in V2-transfected cells following cGAMP treatment (Figures 5A and S5A). Surprisingly, however, in addition to p-dimers and p-hexamers, we also detected p-monomers. Notably, we detected increased p-monomer accumulation in both V2- and V3-transfected cells (Figures 5A, S5A, and S5B), suggesting a functional redundancy between the two isoforms in regulating p-STING monomer accumulation. Disulfide dimers in the absence of cGAMP and p-monomers were also detected with endogenous STING in cGAS$^{-/-}$ BJ cells (Figure S5D).

The above experiments all involved transient expression of the V2/V3 isoforms. We therefore next wished to verify these findings using LOF assays, concentrating on V2, which had the most pronounced effects on STING. We were unable to achieve isoformspecific KD of V2 (or V3), by either small interfering RNA or short hairpin RNA, and therefore employed two different approaches. First, we used the NF-κB inhibitor BMS-345541 employed above to downregulate all WDR33 isoforms (~70%, Figure S5E). Consistent with what we expected based on the above experiments, BMS-345541 treatment of STING-HA-transfected 293T cells increased STING disulfide dimer levels significantly, by ~50%, while correspondingly decreasing monomer levels (Figure 5B). Following cGAMP stimulation, STING disulfide hexamers were also detected at higher levels (~1.6-fold) in BMS-345541-treated cells (Figure 5B). Thus, BMS-345541, which reduces expression of all WDR33 isoforms, induces STING disulfide hyper-oligomerization, consistent with the transient expression experiments described above. However, BMS-345541 of course alters the expression of many genes, and we therefore next examined whether restoration of V2 expression by transient expression (to physiological levels, based on mRNA, Figure S5E) in the BMS345541-treated cells was sufficient to restore levels of STING monomers, dimers, and hexamers to levels detected in untreated cells. This was indeed the case (Figure 5B), indicating that STING hyper-oligomerization induced by BMS-345541 was due, at least in part, to downregulation of V2 expression. Moreover, p-STING monomer levels were also decreased significantly, by ~30%, in BMS-345541-treated cells and were also largely rescued by restoration of V2 expression (Figure 5B).

As a second, and more direct, approach to verify V2 function in STING disulfide oligomerization, we used CRISPR-Cas9 to remove the CDS of the V2 C-terminal TMD in 293T cells without affecting V1 and V3 CDSs (see STAR Methods). We used 293T cells because they are not only well established for studying STING functions[17,24] but are also highly suitable for CRISPR-Cas9 genome editing.[47,48] This generated a V2-dTM mutant protein with one additional serine residue at the C terminus (Figures S5F and S5G). Since V2-dTM is an LOF mutant as described above, the CRISPR-Cas9-edited homozygous clone constitutes an isoform-specific V2 knockout clone (V2-KO). We did not perform V3 KO, both for technical reasons (see STAR Methods) and because it plays a less prominent role in STING regulation than does V2.

We next examined STING protein levels and disulfide oligomerization in STING-HA-transfected V2-KO cells. For this, cells were lysed directly in SDS sample buffer, either under reducing conditions (DTT^{+}) to allow detection of total STING (as monomers) or non-reducing conditions (DTT^{-}) to detect STING disulfide oligomers as well as monomers, and proteins were resolved by SDS-PAGE and analyzed by WB. Not unexpectedly, WT and

V2-KO cells expressed equivalent levels of total STING (Figure 5C, middle right panel, DTT^+). The V2-KO cells, however, displayed strikingly lower (~5-fold) levels of STING monomers and dimers compared to WT cells, with or without cGAMP stimulation (Figure 5C, DTT^-; quantitation on bottom). Hexamers also appeared to be reduced in the V2-KO cells, but levels were low and difficult to quantitate. (Differences in oligomers were more apparent in experiments with native gels described below.) V2-KO cells also displayed significantly (~50%) fewer p-STING monomers following cGAMP stimulation (Figure 5C). The p-monomer fold change was lower than the overall monomer fold change, consistent with the functional redundancy of V2 and V3 in increasing p-monomer accumulation (see above).

To extend these findings, we performed blue native (BN) gel analysis to evaluate STING oligomerization under native states.[17] Similar to the non-reducing denaturing WB results above, STING-HA-transfected V2-KO cells also exhibited strikingly lower levels of STING dimers and oligomers than did WT cells (Figure 5D). We also used the Ser366 p-STING antibody to detect p-STING levels and again detected p-monomers, confirming that STING monomers can indeed be phosphorylated (Figure 5D). Both p-monomer and p-dimer levels were lower in V2-KO cells than in WT cells (Figure 5D). However, despite lower STING oligomer levels in the V2-KO cells, STING p-oligomer levels were similar between V2-KO and WT cells (Figure 5D), indicating that STING oligomers were phosphorylated more efficiently in V2-KO cells. Moreover, even though p-oligomers were detected in WT cells only weakly by non-reducing denaturing WB, they were more abundant when analyzed with BN gels (Figure 5D), suggesting that p-oligomers are not always linked by disulfide bonds.

It is notable that equivalent amounts of total STING protein were present in WT and V2-KO cells, but sharply reduced levels of monomers and oligomers were detected when measured by both non-reducing SDS-PAGE and BN gels. This suggests that there was a significant accumulation of higher-order STING oligomers/polymers in the V2-KO cells compared to WT, and, likely reflecting the hydrophobic nature of the STING TMD, these were unable to enter the gel and/or were entirely insoluble under non-reducing conditions, even in SDS sample buffer.[49] To investigate this possibility, we lysed the cells with Triton/NP-40, separated the extracts into soluble and insoluble fractions, and analyzed them by SDS-PAGE/WB in the presence or absence of DTT (Figure 5E). In the soluble fraction (Supernatant [Sup]), lower levels of STING monomers (and dimers in the absence of DTT) were detected in the V2-KO compared to WT cells, even in the presence of DTT, suggesting that higher-order disulfidelinked oligomers were indeed lost from the soluble fraction. Strikingly, and consistent with this idea, we recovered significant amounts of STING from V2-KO compared to WT cell pellets (Pel), but only under reducing, denaturing conditions. These results confirm that higher-order STING oligomers/polymers were formed in V2-KO cells and were indeed insoluble in the absence of DTT. Overall, our findings demonstrate that in V2-KO cells, STING tends to exist not as monomers or dimers but as large, highly insoluble oligomers/polymers linked by disulfide bonds, indicating that loss of functional V2 leads to STING hyper-oligomerization.

It is also notable that depletion of V2 by BMS-345541 increased STING disulfide dimer/hexamer levels, while V2-KO cells exhibited lower STING oligomer levels. These

apparently contradictory results likely reflect the extent of V2 depletion. BMS-345541-treated cells retained significant amounts of V2 (~30%, based on mRNA, Figure S5E), but functional V2 was completely absent in V2-KO cells. Thus, we suggest, STING oligomerization becomes entirely unregulated by V2 in the V2-KO cells, and STING therefore forms higher-order insoluble oligomers/polymers instead of lower-order oligomers, such as dimers, which were detected in the BMS-345541-treated cells. Overall, however, the results obtained from these two independent LOF assays are entirely consistent with what we observed using the transient expression approach, and confirm that V2 functions as an important regulator of STING oligomerization.

Since STING oligomerization facilitates phosphorylation of TBK1 at Ser172 (p-TBK1),[22] which in turn activates downstream IFNB1 induction,[19] we wondered whether V2 affects p-TBK1 levels. Using the V2 rescue approach, we found that BMS-345541 treatment increased p-TBK1 levels in STINGHA-transfected 293T cells by ~2-fold upon cGAMP stimulation (Figure S5H). Importantly, physiological expression of V2 largely restored p-TBK1 levels to those in untreated cells (Figure S5H). Together, these findings demonstrate that V2 decreases STING disulfide oligomerization, leading to reduced TBK1 phosphorylation, which in turn contributes to decreased IFNB1 induction.

V2 facilitates STING-mediated autophagy

STING also induces autophagy upon cGAMP stimulation.[24,25] We next investigated whether V2 or V3 might be involved in this process. To this end, we first co-transfected STING-HA and 33FLAG-V2 or -V3 into 293T cells and performed WB with an antibody that detects LC3-II, a lipidated protein that serves as a marker for autophagosomes, in the presence or absence of chloroquine (CQ), which inhibits autophagosome-lysosome fusion.[50] In the absence of CQ, a condition under which autophagosomes can be freely degraded, we observed an ~2-fold increase in LC3-II levels in V2-transfected cells compared to EV control cells following cGAMP treatment (Figure 6A). A similar increase was also detected following CQ treatment, which prevents autophagosome degradation, indicating that V2 promotes STING-mediated autophagosome production (Figure 6A). Expression of V3 did not affect LC3-II levels, with or without CQ treatment (Figure S6A), suggesting that only the V2 isoform functions in this process as well as providing further evidence for the specificity of our transient expression results.

We next investigated how V2 promotes autophagy. To do so, we examined the WD protein WIPI2, the earliest known autophagy factor required for STING-induced autophagy.[24] According to RefSeq, there are six annotated WIPI2 isoforms, termed a– f (Figures S6B and 6B). WIPI2b/d, but not WIPI2a/c, are considered the canonical isoforms.[51] Transfection of the WIPI2b plasmid, which produces both the b and d isoforms, caused only a mild increase (~20%) in LC3-II in STING-HA-transfected 293T cells following cGAMP stimulation and CQ treatment (Figure S6C). We next repeated this experiment with WIPI2f, which was of interest because, similar to V2, it lacks multiple WD repeats (Figure 6B). Notably, transfection of the WIPI2f plasmid produced an additional, unannotated isoform, which we named g (Figures 6B and 6C). Expression of WIPI2f/g resulted in a small but significant ~1.5-fold increase in cGAMP-induced LC3-II levels following CQ treatment (Figure 6C).

In light of the results reported above, we investigated the functional relationship between V2 and WIPI2f/g. Given that WIPI2f/g each contain only four WD repeats, they are strong candidates for WDRC. Indeed, by coIP using an FLAG antibody, we detected interaction of 33FLAG-V2 with HA-WIPI2f/g (Figure 6D) but not with HA-WIPI2b/d (Figure S6D). We also examined the effect of V2 and WIPI2f/g on LC3-II levels. Similar to V2/V3 WDRC, co-expression of V2 and WIPI2f/g also led to strong increases in levels of the three proteins (all ~2-fold; Figure S6E). More importantly, we observed a further increase (~35%) in LC3-II levels when these proteins were co-expressed with STING in 293T cells following cGAMP stimulation and CQ treatment (Figure S6E). Additionally, to determine whether the V2 and WIPI2 isoforms are co-regulated, we examined WIPI2 isoform expression upon cGAMP stimulation in cGAS$^{-/-}$ BJ cells. We found that WIPI2f/g, but not WIPI2b/d, mRNA levels were down-regulated by ~50% (Figure 6E), equivalent to what we observed for V2 (see Figure 3B). Thus, V2 and WIPI2f/g likely function together, perhaps via WDRC, to increase the production of autophagosomes.

We next wished to verify V2's function in promoting STINGinduced autophagy by using the two LOF approaches described above. First, BMS-345541 treatment of STING-HA-transfected 293T cells significantly reduced LC3-II levels, by ~50%, following cGAMP stimulation, with or without CQ (Figure 6F). Importantly, however, restoration of V2 expression, again to physiological levels, restored LC3-II levels, indicating that the lower autophagic activity in BMS-345541-treated cells was due at least in part to reduced V2 expression (Figure 6F). This effect of V2 on LC3-II levels was entirely STING dependent, as no differences were observed in the absence of STING (Figure S6F). We next examined LC3-II levels in V2-KO cells. Surprisingly, we detected a ~2-fold increase in cGAMP-induced LC3-II levels in STING-HA-transfected V2-KO cells compared to WT, with or without CQ (Figure S6G). This appeared to contradict findings from both our transient expression and V2 rescue experiments. To investigate the possible cause, we examined mRNA expression of WIPI2 isoforms in V2-KO cells by RT-qPCR. Strikingly, we found that WIPI2b/d and WIPI2f/g mRNA levels were increased, by ~2-fold and ~4-fold, respectively (Figure S6H). These findings suggest that the increased autophagosome production in V2-KO cells was likely due to increased WIPI2 expression, revealing an unexpected compensatory mechanism for loss of V2.

V2 and V3 emerged after STING

Finally, given that cGAS and STING co-evolved,[52,53] we were interested in determining the evolutionary relationship between V2/V3 and STING. Both V2 and V3 are only annotated for some vertebrates, so we manually examined the *Wdr33* genes of several invertebrates and were able to identify V2 homologs in *D. melanogaster* and *N. vectensis*. No invertebrate V3 homologs were found. These homologs are also produced by APA, and the proteins are also predicted to contain only the first two WD repeats and to harbor C-terminal TMDs (Figure S7A). Examination of conservation patterns of STING, WDR33 isoforms, autophagy, interferons, and NF-κB in several organisms revealed that STING emerged before V2, and V2 emerged before V3 (Figure S7B). V2 appeared to co-evolve with NF-κB, and V3 appeared to co-evolve with interferons (Figure S7B). Notably, *C. elegans* is known to have lost the cGAS-STING pathway during evolution,[52,53] and we did not find a *C.*

elegans V2 homolog (Figure S7B). These analyses provide further evidence that V2 and V3 are functionally related to STING.

DISCUSSION

In this study, we have shown that two isoforms of the well-studied core nuclear mRNA polyadenylation factor WDR33, produced by APA, are not themselves polyadenylation factors but instead localize to the ER and function in STING-mediated innate immune responses. To our knowledge, there is only one other example in which alternative mRNA processing gives rise to protein isoforms with completely unrelated functions. In that case, an isoform produced by a combination of AS and APA of transcripts from the *CUX1* gene, which itself encodes a transcription factor, was shown to encode a Golgi membrane protein.[54] It is notable that WDR33 and CUX1 are similar in the sense that a non-canonical isoform of a nuclear protein is a transmembrane protein, although the significance of this, if any, is unknown. In any event, our findings highlight how the coding potential of the human genome can be expanded by using the same sequence information to produce proteins with entirely distinct functions and that this can be achieved solely via APA.

Our analyses of WDR33 APA identified an interesting mode of exonic APA. V2 PAS0 is within its CDS, and usage of this site produces an mRNA lacking a 3′ UTR. A similar mode of CDS APA has been reported previously.[55] PAS3, however, is located within exon 7, and its usage unexpectedly causes retention of intron 6. Nazim et al. reported that usage of a PAS within alternative exon 5 of the human acetylcholinesterase (AChE) pre-mRNA causes retention of intron 4.[56] However, the AChE exonic PAS is far downstream of intron 4 (~350 nt), in contrast to V2 PAS3, which is only 16 nt away from the intron 6 3′ SS, indicating that these are likely two distinct mechanisms. Intron 6 retention by PAS3 usage could be due to blockage of the 3′ SS by the CPA machinery.

Our study has revealed unexpected insights into STING function and regulation. We found that V2 suppresses STING disulfide bond-mediated oligomerization, possibly by preventing Cys148 disulfide bond formation through direct protein-protein interaction.[17] This function of V2 has the potential to be of considerable importance. For example, uncontrolled STING activation, which could be caused by the hyper-oligomerization we observed in the absence of V2 in the V2-KO cells, can lead to autoimmune diseases, including Aicardi-Goutières syndrome[57] and STING-associated vasculopathy with onset in infancy.[58] Further studies to investigate the possible role of V2 in these diseases, and in the regulation of STING oligomerization more generally, will be informative.

In canonical autophagy, WIPI2 recruits the ATG12-5-16L complex through its WD repeats 2 and 3.[59,60] These two repeats are missing in WIPI2f/g. Thus, an interesting possibility is that V2 contributes its two WD repeats, by the WDRC mechanism we proposed, for recruitment of the downstream factors. It should be noted that we do not rule out roles for WIPI2b/d in STING-induced autophagy, and indeed Wan et al. demonstrated recently that STING interacts directly with WIPI2 (the exact isoform was not specified).[26] Our findings that WIPI2f/g also promote cGAMP-induced autophagosome production, possibly by interacting with V2, and that WIPI2b/d/f/g are all upregulated in V2-KO cells, suggest that STING can

induce autophagy in multiple ways. It will also be of interest to determine the mechanism by which loss of V2 leads to upregulation of WIPI2 isoforms, which our data show occurs at the transcript level.

We also unexpectedly detected phosphorylated STING monomers and showed that their accumulation can be promoted by both V2 and V3 expression and decreased by V2-KO. These findings, however, seem inconsistent with those of Zhang et al., who suggested, based on structural data, that oligomerization of both TBK1 and STING is required for STING phosphorylation.[22] However, Zhang et al. also reported that the direct binding between TBK1 and STING was flexible and variable *in vitro*.[22] It is possible that an additional protein that bridges STING and TBK1 was missing from their structures. Given that WD proteins generally facilitate protein-protein interactions,[61] we suggest that V2/V3 can facilitate TBK1-STING interaction, allowing the phosphorylation of STING monomers by TBK1.

Our discovery of p-monomers potentially reconciles two longstanding opposing views regarding the function of Ser366 phosphorylation. Liu et al. suggested that Ser366 phosphorylation by TBK1 is required for IFNB1 induction.[20] Konno et al., however, had previously reported that a phosphomimetic S366D STING mutant activated the NF-κB pathway but failed to induce IFNB1.[62] We suggest that this S366D mutant mimics p-monomers, as opposed to p-oligomers, and as a result our findings that V2 increases accumulation of p-monomers and suppresses IFNB1 but not IL-6 are entirely consistent with the findings of Konno et al.[62] STING monomer phosphorylation thus likely serves as an inhibitory regulation of IFNB1 induction.

It is of interest that V2 and V3 mRNA levels were increased similarly following poly(I:C) but were reduced, and again to the same extent, following cGAMP treatment. These results suggest that V2/V3 might play distinct roles in different types of immune responses. Different immune stimuli or different cell types may differentially regulate V2/V3 expression. Indeed, as reported by Miller et al., IAV infection decreases V2, but does not affect V1 or V3, expression.[36] Recently, Wilton et al. reported an increase in V2, but not V1 or V3, in primary human macrophages as they were polarized into a pro-inflammatory state or were co-cultured with cancer cells.[63] This finding also suggests that V2 might contribute to macrophage anti-tumor activity. This is not surprising, given that V2 can increase autophagic activity and that autophagy regulates many macrophage functions, such as antigen presentation[64] and several other functions.[65] V2 might then also play a role in macrophage accumulation at tumor sites, which can be STING dependent.[66] It will thus be of interest to expand our current findings of V2/V3 regulation and function in future studies in more complex systems, such as V2/V3 transgenic mice.

Based on our findings, we propose the following model for V2 in STING-mediated immune responses. When V2 expression is low, STING can freely form disulfide oligomers upon cGAMP activation, efficiently inducing IFNB1 (Figure 7Ai). A fraction of STING molecules exists as monomers due to their interaction with V2, which recruits WIPI2f/g for autophagy induction (Figure 7Aii). However, when highly expressed, V2 prevents accumulation of STING disulfide-linked oligomers, thereby decreasing IFNB1 induction

(Figure 7Bi). Levels of STING monomers are in turn increased, allowing V2 to recruit more WIPI2f/g to promote autophagosome production (Figure 7Bii). The role of V3 seems less significant, and it does not function in autophagy at all.

In summary, our study has shown that V2 and V3, non-canonical isoforms of the polyadenylation factor WDR33, are regulators of STING-mediated innate immune responses. Arising from IPA and a splicing-modulating form of APA, V2 localizes to the ER and interacts with STING to prevent STING oligomerization and reduce IFNB1 induction while also functioning to promote autophagy. V3, on the other hand, also localizes to the ER and appears to increase STING levels, perhaps by inhibiting V2 via a proteinprotein interaction mechanism we described termed WDRC. Our study thus not only provides unexpected insights into regulation of STING-mediated immune responses but also demonstrates that alternative mRNA processing is a more powerful mechanism than previously appreciated, allowing production of proteins with totally different functions from the same gene.

Limitations of the study

While we have provided multiple lines of evidence that V2 exists as a protein, endogenous V2/V3 protein levels remain unclear, due to the lack of appropriate antibodies. WDRC was studied by coIP and requires structure determination to be characterized fully. We relied on exogenous expression of STING in 293T cells to study V2/V3 functions in STING regulation. While this is a well-established system to study STING,[17,19,20,24,62] and, as noted throughout the article, exogenous STING functioned properly in all our assays, complementary studies with endogenous STING will be of value. LOF assays were performed using BMS-345541 and by generation of an endogenous V2-KO mutant. While these approaches have confirmed the role of V2 in STING regulation, it is possible that BMS-345541 also affects other genes that function with STING and that the V2-KO mutant affects other cellular processes.

STAR★METHODS

RESOURCE AVAILABILITY

Lead contact—Further information and requests for resources and reagents should be directed to and will be fulfilled by the lead contact, James L. Manley (jlm2@columbia.edu).

Materials availability—Materials and reagents generated in this study are available from the lead contact upon request.

Data and code availability

- This paper analyzes existing, publicly available data. Accession numbers for the datasets are listed in the key resources table.
- This paper does not report original code.
- Any additional information required to reanalyze the data reported in this paper is available from the lead contact upon request.

EXPERIMENTAL MODEL AND STUDY PARTICIPANT DETAILS

All experiments were performed using cultured human cell lines. Human cervical cancer HeLa (female), human embryonic kidney 293T (female), human osteosarcoma U2OS (female) and human glioblastoma U87 (male) were obtained from ATCC. H9 human embryonic stem cells (female)[68] were obtained in a previous study from our lab.[27] cGAS$^{-/-}$ immortalized human foreskin fibroblast BJ-5ta (male)[38] were described in Ng et al.[39] WDR33v2$^{dTM/dTM}$ (V2-KO) 293T cells were generated in this study. All cells were cultured at 37°C with 5% CO_2, and were passaged every 3–4 days. Experiments were performed on cells with no more than 20 passages after thawing. Morphologies of cells were consistent with those described by ATCC. Growth rate of V2-KO cells did not deviate significantly from the parental cells.

METHOD DETAILS

Cell culture—HeLa, 293T, U2OS and U87 cells were cultured in DMEM supplemented with 10% FBS. H9 hESCs were cultured in Essential 8 medium (Stem Cell Technologies) on Matrigel (Corning)-coated plates. Derivation of EBs is described in Yamazaki et al.[27] Briefly, H9 cells were first dissociated using ReLeSR (Stem Cell Technologies), and were then resuspended in EB medium (DMEM/F12, 15% FBS, 15% knock-out serum, 0.1 mM nonessential amino acid, and 0.5% penicillin and streptomycin) on the Nunclon Sphera (Thermo Scientific) dishes. cGAS$^{-/-}$ BJ cells were cultured in a 4:1 mixture of DMEM and Medium 199 (Gibco) supplemented with 10% FBS and 10 μg/mL hygromycin.

Molecular cloning—WDR33v2 (GenBank: NM_001006622), WDR33v3 (GenBank: NM_001006623), EMD (GenBank: NM_000117), CANX (GenBank: NM_001746), STING (GenBank: NM_198282), and WIPI2b (GenBank: NM_016003)/f (GenBank: NM_001278299) CDSs were directly amplified by PCR. For WDR33v1 (GenBank: NM_018383), the ~4 kb CDS was separately amplified as four ~1-kb pieces and assembled together using overlapping extension PCR. The V2-dTM mutant plasmid was derived from wildtype V2 plasmid. Vector backbones used were pcDNA3 and pCXS (for V2, V3 and WIPI2b/d/f/g). pCXS was derived from the pCXLE plasmid[75] (Addgene #27082) by removing the EBNA1 episomal cassette. WDR33v1-transformed bacteria were cultured at room temperature (RT). The STING plasmid was subjected to site-directed mutagenesis to produce the Arg232 variant, which is considered “wildtype”.[76] All plasmids were sequenced to ensure that there were no mutations.

Transfection—For 293T and HeLa cells, DNA transfection was performed using Lipofectamine 2000 (Invitrogen). For BJ cells, GeneXPlus transfection reagent (ATCC) was used. Transfected BJ cells were cultured in medium containing 20% FBS for the first 24 h. We have performed RT-qPCR to quantify expression of exogenous V2 and V3 mRNAs in 293T cells under maximal plasmid levels, and observed ~8-fold increase in total V2 mRNA levels in V2-transfected cells (Figure S2B). V3-transfected cells, on the other hand, exhibited more than 150-fold increase in V3 mRNA levels, likely owing to its low endogenous levels (Figure S2B). In several experiments, we included samples transfected with less plasmid (Figures 4B–4D and S4A–S4C), created an expression gradient (Figures 5A, S5A, and S5B) or used 50% of the amount of plasmid for co-expression (Figures

2C, 2D, S2C, S2D, and S6E). In these experiments, exogenous V2 mRNA levels were expected to be much lower. We did not examine exogenous V2 and V3 mRNA levels in transfected HeLa or BJ cells, but exogenous expression in these cells was likely much lower than in 293T cells, as 293T cells are more transfectable, especially compared to BJ cells. For V2 rescue experiments (Figures 5B, S5E, and 6F), the amount of V2 plasmid used to restore V2 expression was much lower than what was used for transient expression functional assays, and insufficient to affect STING functions in these assays. To ensure that V2/V3 transfection did not induce ER stress that could affect STING functions, we examined ER stress by RT-qPCR in transfected cells according to Oslowski et al.[77] We did not detect induction of ER stress markers BiP, ATF4 and GRP94 (Figure S7C). siRNAs were transfected using DharmaFECT 1 (Dharmacon). siIRF3 sequence was from Jiao et al.[69] Non-targeting negative control siRNAs were from Sigma-Aldrich.

Immune stimulation and drug treatment—Poly(I:C) (Tocris) dissolved in 0.9% NaCl was introduced into HeLa cells using Lipofectamine 2000 at 500 ng/mL for 6 h. cGAMP (Invivogen) was delivered into cells either by direct treatment at the indicated concentrations and durations or by digitonin permeabilization.[78] For digitonin permeabilization, cells were incubated with the permeabilization buffer (50 mM HEPES, 100 mM KCl, 3 mM MgCl2, 0.1 mM DTT, 85 mM sucrose, 0.2% BSA, 1 mM ATP, 0.1 mM GTP, and 10 μg/mL digitonin) with or without cGAMP at 4 μM for 30 min at 37°C. The permeabilization buffer was then replaced with fresh DMEM, and the cells were further incubated at 37°C for 3 h before harvest. Interferon-β (Bio-Techne) was dissolved in 10 mM citric acid, 1% BSA, and 0.5% CHAPS. Dissolved interferon-β was diluted in DMEM at 10 ng/mL for direct treatment for 24 h. MG132 (MedChemExpress) treatment was carried out at 20 μM for 12 h. BMS-345541 (Adooq Bioscience) treatment was performed at 50 μM for 1 h prior to and during poly(I:C) or cGAMP stimulation, or for a total of 7 h for rescue experiments. For chloroquine (Sigma-Aldrich) treatment, cells were incubated with the drug at 50 μM for 30 min prior to cGAMP stimulation, during the stimulation, and during the post-stimulation incubation for a total of 4 h.

cDNA synthesis, PCR and 3′RACE—Total RNA was extracted using Trizol (Ambion). Raji cell RNA samples were from Yamazaki et al.[67] cDNA was synthesized using the Maxima reverse transcriptase (Thermo Scientific) and the random hexamer primer (Invitrogen). qPCR was performed using SYBR Green PCR Master Mix (Applied Biosystems) on the StepOnePlus qPCR system (Applied Biosystems). qPCR data were analyzed using the $-\Delta\Delta C_T$ method. RPL13a was used as the endogenous control for hESC differentiation samples.[79] GAPDH was used as the endogenous control for immune experiments.[80] 3′RACE was performed according to Scotto-Lavino et al.[81] Briefly, cDNA was synthesized using the oligo(dT) primer (QT) containing two tandem adaptors at the 5′ end. The first PCR reaction was performed using a PAS-specific primer and the outer adaptor primer (QO). Products were diluted 20 times and were used as the templates for the second PCR reaction, where another PAS-specific primer downstream of the first one and the inner adaptor primer (QI) were used. Since different primer pairs were used for different PASs, band intensities are not comparable between PASs in Figure 1D. The final

PCR products were sequenced to ensure specificity of the reactions. Primer sequences are listed in Table S2.

Western blot—Unless otherwise noted, protein samples were directly lysed in SDS sample buffer. 100 mM DTT was included in samples designated for reducing WB, and the samples were boiled for 5 min before loading onto a gel. For non-reducing WB, DTT was omitted from the sample buffer, and samples were not boiled. Instead, samples were passed through a 20G syringe needle 12 times on ice to shear genomic DNA. To detect insoluble STING oligomers/polymers, cells were first lysed in IP buffer containing Triton and NP-40 (see Coimmunoprecipitation section below). Lysates were then rotated at 4°C for 15 min followed by a centrifugation at 15000 rpm for 15 min. Equal volume of 2X SDS sample buffer with or without DTT was added to the supernatants. The pellets were resuspended in 1X SDS sample buffer with or without DTT. The final volumes of the supernatant and pellet samples were the same. Proteins were separated in 10% SDS-PAGE and transferred for 90 min at 90 V to a nitrocellulose membrane (0.45 μm pore) using standard transfer buffer (10% methanol). For LC3 WB, 14% SDS-PAGE was used, and proteins were transferred using buffer containing 20% methanol to a nitrocellulose membrane (0.2 μm pore) for 90 min at 90 V. Membranes were blocked in 4% non-fat milk or 2% BSA (for p-STING) in 0.1% tween in PBS/TBS (for phosphorylated antigens). After blocking, membranes were incubated with primary antibodies diluted in the blocking buffer overnight at 4°C. After three washes with 0.1% tween in PBS/TBS, membranes were incubated with the appropriate HRP-conjugated secondary antibodies (Sigma-Aldrich) diluted in the blocking buffer for 1 h at RT. ECL (Kindle Biosciences) chemiluminescence signals were detected using the ChemiDoc MP Imaging System (Bio-Rad). GAPDH was used as the endogenous loading control.

Blue native gel—Blue native PAGE was performed using a modified protocol based on Ergun et al.[17] Mock-or cGAMP-treated STING-transfected WT and V2-KO cells were lysed in a buffer containing 10% glycerol, 25mM NaCl, 20mM HEPES pH 7.0 and 1% Triton, with protease and phosphatase inhibitors. After clearing the lysates, Coomassie brilliant blue G250 was added to the lysates at an 8:1 detergent/G250 ratio.[82] Samples were loaded onto a PAGE gel without SDS and electrophoresis was performed at 4°C, followed by regular western blot procedures described above.

Co-immunoprecipitation—Confluent transfected 293T cells on 10-cm dishes were lysed in IP buffer (50 mM Tris-Cl, pH 7.4, 150 mM NaCl, 1 mM EDTA, 1% Triton X-100, 01% NP-40, and 1X protease inhibitor cocktail (Bimake)). For cells treated with cGAMP, phosphatase inhibitor cocktail (Bimake) was also included. RNase A (Sigma-Aldrich) was always added to the cell lysates to eliminate potential RNA-mediated interactions. After saving 10% lysates as inputs, the remaining cell lysates were mixed with anti-FLAG antibody (Sigma-Aldrich, F1804) and rotated at 4°C overnight. Next day, the mixtures were incubated with protein A/G magnetic beads (Thermo Scientific) at 4°C with rotations for 3 h. After four washes with 0.1% Triton/TBS, proteins were eluted either by directly boiling the beads in SDS sample buffer for 5 min or by incubating in 0.1 M Glycine pH 2 for 10 min at RT.

Immunofluorescence—293T cells seeded on coverslips were fixed using ice-cold 4% paraformaldehyde in PBS for 15 min at RT. For Triton pre-extraction, living cells were treated with pre-extraction buffer (1% Triton X-100, 10 mM Tris-Cl pH 7.5, 1.5 mM $MgCl_2$, 2 mM $CaCl_2$) for 30 s at RT before fixation.[8] 0.1% Triton/PBS was used to permeabilized cells for 5 min. Cells were blocked in 10% goat serum (Sigma-Aldrich) in PBS for 1 h at RT. Subsequently, cells were incubated with primary antibodies diluted in blocking buffer either for 1 h at RT or overnight at 4°C. Following three PBS washes, cells were incubated with Alexa Fluor Secondary Antibodies (Invitrogen) diluted in 0.1% Triton/PBS for 1 h at RT. The coverslips were mounted onto microscope slides with mounting medium containing DAPI (Abcam). Imaging was performed using the LSM700 Confocal Microscope (Zeiss) under the 63X objective lens. For Triton pre-extracted 293T and BJ, cells were imaged using the Nikon Eclipse Ts2-R FL Inverted Fluorescence Microscope (Nikon) under the 20X and 5X objective lenses, respectively.

CRISPR/Cas9 genome editing—The *WDR33* gene in 293T cells was edited according to Ran et al.[47] gRNAs targeting the vicinities of the 5′ or 3′ ends of intron 6 were cloned into PX458 (Addgene #48138, with eGFP) or PX459 V2.0 (Addgene #62988, with puromycin resistance). The plasmids were transfected into 293T cells, and puromycin selection was performed 24 h after transfection for 3 days. Single clones were selected, screened by RT-PCR genotyping and confirmed by sequencing (see Figures S5F and S5G). The 5′ and 3′ gRNA sequences are listed in the key resources table. These two gRNAs removed a ~1.5 kb region of *WDR33* intron 6, which contains the CDS of V2 TMD. We did not perform V3 KO, because V3 does not contain a unique functional domain like V2, and the associated intron 7 is too large (>36 kb) to remove and likely contains many cryptic polyadenylation sites.

Bioinformatic and RNA-seq analyses—Transmembrane prediction was performed using TMHMM 2.0[33] and TMPred.[34] Hydrophobicity plot was generated by TMPred, and transmembrane probability plots were generated by TMHMM. Ribosome profiling dataset of 293 cells (GSE112353) was generated by Clamer et al.[31] HeLa (GSE123105) and A549 (GSE147507) RNA-seq datasets were generated by Kamieniarz-Gdula et al.[29] and Blanco-Melo et al.,[30] respectively. RNA-seq reads were first subjected to quality control and adaptor trimming by Cutadapt.[71] Afterward, they were pseudo-aligned to the GENCODE human transcriptome (GRCh38.p13)[74] using kallisto, which specializes in RNA quantification at the transcript level.[72] The TPM numbers obtained from kallisto were used for within-sample abundance comparison between WDR33 transcript variants and for detection of V1, V2 and V3 mRNAs' association with ribosomes. Quantification results from kallisto were imported into sleuth on R for transcript-level differentiation expression analyses.[73] Analyses were run according to developers' recommendations and sample preparation provided by the depositors of the original data.

QUANTIFICATION AND STATISTICAL ANALYSIS

Band intensityes from WB and RT-PCR gels were quantified by FIJI ImageJ[70] and normalized to endogenous control intensities. For autophagy western blots, LC3-II levels normalized to GAPDH were analyzed (LC3-I levels should not be used to evaluate

autophagy[83]).Pairwise comparison was performed using Student's t-test on Microsoft Office Excel. For qPCR data, t test was performed on ΔC_T. $p < 0.05$ was considered statistically significant. For transcript-level differential expression analyses using sleuth, the built-in Wald test option was used. FDR <0.05 was considered statistically significant. All statistical analyses were performed on data obtained from three experiments.

Supplementary Material

Refer to Web version on PubMed Central for supplementary material.

ACKNOWLEDGMENTS

We thank Takashi Yamazaki for technical advice, Takahiro Seimiya for help with maintaining/screening CRISPR-Cas9-edited cells, and Manley lab members for discussions. We also thank Zhijian Chen (University of Texas Southwestern Medical Center), Hachung Chung (Columbia University Irving Medical Center), Liang Tong (Columbia University), and Marko Jovanovic (Columbia University) for comments and feedback. We thank Pamela Silver (Harvard Medical School) for cGAS$^{-/-}$ BJ cells. L.L. was supported in part by the US NSF Graduate Research Fellowship (DGE-2036197). This work was supported by National Institutes of Health R35 GM118136 (to J.L.M.).

REFERENCES

1. Shi Y, Di Giammartino DC, Taylor D, Sarkeshik A, Rice WJ, Yates JR 3rd, Frank J, and Manley JL (2009). Molecular architecture of the human pre-mRNA 3' processing complex. Mol. Cell 33, 365–376. [PubMed: 19217410]
2. Sun Y, Hamilton K, and Tong L (2020). Recent molecular insights into canonical pre-mRNA 3'-end processing. Transcription 11, 83–96. [PubMed: 32522085]
3. Chan SL, Huppertz I, Yao C, Weng L, Moresco JJ, Yates JR 3rd, Ule J, Manley JL, and Shi Y (2014). CPSF30 and Wdr33 directly bind to AAUAAA in mammalian mRNA 3' processing. Genes Dev. 28, 2370–2380. [PubMed: 25301780]
4. Schönemann L, Kühn U, Martin G, Schaöfer P, Gruber AR, Keller W, Zavolan M, and Wahle E (2014). Reconstitution of CPSF active in polyadenylation: recognition of the polyadenylation signal by WDR33. Genes Dev. 28, 2381–2393. [PubMed: 25301781]
5. Clerici M, Faini M, Muckenfuss LM, Aebersold R, and Jinek M (2018). Structural basis of AAUAAA polyadenylation signal recognition by the human CPSF complex. Nat. Struct. Mol. Biol 25, 135–138. [PubMed: 29358758]
6. Sun Y, Zhang Y, Hamilton K, Manley JL, Shi Y, Walz T, and Tong L (2018). Molecular basis for the recognition of the human AAUAAA polyadenylation signal. Proc. Natl. Acad. Sci. USA 115, E1419–E1428. [PubMed: 29208711]
7. O'Leary NA, Wright MW, Brister JR, Ciufo S, Haddad D, McVeigh R, Rajput B, Robbertse B, Smith-White B, Ako-Adjei D, et al. (2016). Reference sequence (RefSeq) database at NCBI: current status, taxonomic expansion, and functional annotation. Nucleic Acids Res. 44, D733–D745. [PubMed: 26553804]
8. Schirmer EC, Florens L, Guan T, Yates JR 3rd, and Gerace L (2003). Nuclear membrane proteins with potential disease links found by subtractive proteomics. Science 301, 1380–1382. [PubMed: 12958361]
9. Derti A, Garrett-Engele P, Macisaac KD, Stevens RC, Sriram S, Chen R, Rohl CA, Johnson JM, and Babak T (2012). A quantitative atlas of polyadenylation in five mammals. Genome Res. 22, 1173–1183. [PubMed: 22454233]
10. Hoque M, Ji Z, Zheng D, Luo W, Li W, You B, Park JY, Yehia G, and Tian B (2013). Analysis of alternative cleavage and polyadenylation by 3' region extraction and deep sequencing. Nat. Methods 10, 133–139. [PubMed: 23241633]
11. Tian B, and Manley JL (2017). Alternative polyadenylation of mRNA precursors. Nat. Rev. Mol. Cell Biol 18, 18–30. [PubMed: 27677860]

12. Mitschka S, and Mayr C (2022). Context-specific regulation and function of mRNA alternative polyadenylation. Nat. Rev. Mol. Cell Biol 23, 779–796. [PubMed: 35798852]
13. Zhang X, Bai XC, and Chen ZJ (2020). Structures and Mechanisms in the cGAS-STING Innate Immunity Pathway. Immunity 53, 43–53. [PubMed: 32668227]
14. Ritchie C, Carozza JA, and Li L (2022). Biochemistry, Cell Biology, and Pathophysiology of the Innate Immune cGAS-cGAMP-STING Pathway. Annu. Rev. Biochem 91, 599–628. [PubMed: 35287475]
15. Sun L, Wu J, Du F, Chen X, and Chen ZJ (2013). Cyclic GMP-AMP synthase is a cytosolic DNA sensor that activates the type I interferon pathway. Science 339, 786–791. [PubMed: 23258413]
16. Wu J, Sun L, Chen X, Du F, Shi H, Chen C, and Chen ZJ (2013). Cyclic GMP-AMP is an endogenous second messenger in innate immune signaling by cytosolic DNA. Science 339, 826–830. [PubMed: 23258412]
17. Ergun SL, Fernandez D, Weiss TM, and Li L (2019). STING Polymer Structure Reveals Mechanisms for Activation, Hyperactivation, and Inhibition. Cell 178, 290–301.e10. [PubMed: 31230712]
18. Ishikawa H, Ma Z, and Barber GN (2009). STING regulates intracellular DNA-mediated, type I interferon-dependent innate immunity. Nature 461, 788–792. [PubMed: 19776740]
19. Tanaka Y, and Chen ZJ (2012). STING specifies IRF3 phosphorylation by TBK1 in the cytosolic DNA signaling pathway. Sci. Signal 5, ra20. [PubMed: 22394562]
20. Liu S, Cai X, Wu J, Cong Q, Chen X, Li T, Du F, Ren J, Wu YT, Grishin NV, and Chen ZJ (2015). Phosphorylation of innate immune adaptor proteins MAVS, STING, and TRIF induces IRF3 activation. Science 347, aaa2630. [PubMed: 25636800]
21. Stempel M, Chan B, Juranić Lisnić V, Krmpotić A, Hartung J, Paludan SR, Füllbrunn N, Lemmermann NA, and Brinkmann MM (2019). The herpesviral antagonist m152 reveals differential activation of STINGdependent IRF and NF-κB signaling and STING's dual role during MCMV infection. EMBO J. 38, e100983. [PubMed: 30696688]
22. Zhang C, Shang G, Gui X, Zhang X, Bai XC, and Chen ZJ (2019). Structural basis of STING binding with and phosphorylation by TBK1. Nature 567, 394–398. [PubMed: 30842653]
23. Dikic I, and Elazar Z (2018). Mechanism and medical implications of mammalian autophagy. Nat. Rev. Mol. Cell Biol 19, 349–364. [PubMed: 29618831]
24. Gui X, Yang H, Li T, Tan X, Shi P, Li M, Du F, and Chen ZJ (2019). Autophagy induction via STING trafficking is a primordial function of the cGAS pathway. Nature 567, 262–266. [PubMed: 30842662]
25. Liu D, Wu H, Wang C, Li Y, Tian H, Siraj S, Sehgal SA, Wang X, Wang J, Shang Y, et al. (2019). STING directly activates autophagy to tune the innate immune response. Cell Death Differ. 26, 1735–1749. [PubMed: 30568238]
26. Wan W, Qian C, Wang Q, Li J, Zhang H, Wang L, Pu M, Huang Y, He Z, Zhou T, et al. (2023). STING directly recruits WIPI2 for autophagosome formation during STING-induced autophagy. EMBO J. 42, e112387. [PubMed: 36872914]
27. Yamazaki T, Liu L, Lazarev D, Al-Zain A, Fomin V, Yeung PL, Chambers SM, Lu CW, Studer L, and Manley JL (2018). TCF3 alternative splicing controlled by hnRNP H/F regulates E-cadherin expression and hESC pluripotency. Genes Dev. 32, 1161–1174. [PubMed: 30115631]
28. Ito S, Sakai A, Nomura T, Miki Y, Ouchida M, Sasaki J, and Shimizu K (2001). A novel WD40 repeat protein, WDC146, highly expressed during spermatogenesis in a stage-specific manner. Biochem. Biophys. Res. Commun 280, 656–663. [PubMed: 11162572]
29. Kamieniarz-Gdula K, Gdula MR, Panser K, Nojima T, Monks J, Wiśniewski JR, Riepsaame J, Brockdorff N, Pauli A, and Proudfoot NJ (2019). Selective Roles of Vertebrate PCF11 in Premature and FullLength Transcript Termination. Mol. Cell 74, 158–172.e9. [PubMed: 30819644]
30. Blanco-Melo D, Nilsson-Payant BE, Liu WC, Uhl S, Hoagland D, Møller R, Jordan TX, Oishi K, Panis M, Sachs D, et al. (2020). Imbalanced Host Response to SARS-CoV-2 Drives Development of COVID-19. Cell 181, 1036–1045.e9. [PubMed: 32416070]

31. Clamer M, Tebaldi T, Lauria F, Bernabò P, Gómez-Biagi RF, Marchioretto M, Kandala DT, Minati L, Perenthaler E, Gubert D, et al. (2018). Active Ribosome Profiling with RiboLace. Cell Rep. 25, 1097–1108.e5. [PubMed: 30355487]
32. Afanasieva E, Chaudhuri I, Martin J, Hertle E, Ursinus A, Alva V, Hartmann MD, and Lupas AN (2019). Structural diversity of oligomeric β-propellers with different numbers of identical blades. Elife 8, e49853. [PubMed: 31613220]
33. Krogh A, Larsson B, von Heijne G, and Sonnhammer EL (2001). Predicting transmembrane protein topology with a hidden Markov model: application to complete genomes. J. Mol. Biol 305, 567–580. [PubMed: 11152613]
34. Hofmann K, and Stoffel W (1993). TMbase-a database of membrane spanning proteins segments. Biol. Chem. Hoppe Seyler 347, 166.
35. Brass AL, Huang IC, Benita Y, John SP, Krishnan MN, Feeley EM, Ryan BJ, Weyer JL, van der Weyden L, Fikrig E, et al. (2009). The IFITM proteins mediate cellular resistance to influenza A H1N1 virus, West Nile virus, and dengue virus. Cell 139, 1243–1254. [PubMed: 20064371]
36. Miller MS, Rialdi A, Ho JSY, Tilove M, Martinez-Gil L, Moshkina NP, Peralta Z, Noel J, Melegari C, Maestre AM, et al. (2015). Senataxin suppresses the antiviral transcriptional response and controls viral biogenesis. Nat. Immunol 16, 485–494. [PubMed: 25822250]
37. Akira S, Uematsu S, and Takeuchi O (2006). Pathogen recognition and innate immunity. Cell 124, 783–801. [PubMed: 16497588]
38. Bodnar AG, Ouellette M, Frolkis M, Holt SE, Chiu CP, Morin GB, Harley CB, Shay JW, Lichtsteiner S, and Wright WE (1998). Extension of life-span by introduction of telomerase into normal human cells. Science 279, 349–352. [PubMed: 9454332]
39. Ng TL, Olson EJ, Yoo TY, Weiss HS, Koide Y, Koch PD, Rollins NJ, Mach P, Meisinger T, Bricken T, et al. (2022). High-Content Screening and Computational Prediction Reveal Viral Genes That Suppress the Innate Immune Response. mSystems 7, e0146621. [PubMed: 35319251]
40. Suter MA, Tan NY, Thiam CH, Khatoo M, MacAry PA, Angeli V, Gasser S, and Zhang YL (2021). cGAS-STING cytosolic DNA sensing pathway is suppressed by JAK2-STAT3 in tumor cells. Sci. Rep 11, 7243. [PubMed: 33790360]
41. Luecke S, Sheu KM, and Hoffmann A (2021). Stimulus-specific responses in innate immunity: Multilayered regulatory circuits. Immunity 54, 1915–1932. [PubMed: 34525335]
42. Zamorano Cuervo N, and Grandvaux N (2020). ACE2: Evidence of role as entry receptor for SARS-CoV-2 and implications in comorbidities. Elife 9, e61390. [PubMed: 33164751]
43. Burke JR, Pattoli MA, Gregor KR, Brassil PJ, MacMaster JF, McIntyre KW, Yang X, Iotzova VS, Clarke W, Strnad J, et al. (2003). BMS-345541 is a highly selective inhibitor of IκB kinase that binds at an allosteric site of the enzyme and blocks NF-κB-dependent transcription in mice. J. Biol. Chem 278, 1450–1456. [PubMed: 12403772]
44. Mikuda N, Kolesnichenko M, Beaudette P, Popp O, Uyar B, Sun W, Tufan AB, Perder B, Akalin A, Chen W, et al. (2018). The IκB kinase complex is a regulator of mRNA stability. EMBO J. 37, e98658. [PubMed: 30467221]
45. Ishikawa H, and Barber GN (2008). STING is an endoplasmic reticulum adaptor that facilitates innate immune signalling. Nature 455, 674–678. [PubMed: 18724357]
46. Dobbs N, Burnaevskiy N, Chen D, Gonugunta VK, Alto NM, and Yan N (2015). STING Activation by Translocation from the ER Is Associated with Infection and Autoinflammatory Disease. Cell Host Microbe 18, 157–168. [PubMed: 26235147]
47. Ran FA, Hsu PD, Wright J, Agarwala V, Scott DA, and Zhang F (2013). Genome engineering using the CRISPR-Cas9 system. Nat. Protoc 8, 2281–2308. [PubMed: 24157548]
48. Giuliano CJ, Lin A, Girish V, and Sheltzer JM (2019). Generating Single Cell-Derived Knockout Clones in Mammalian Cells with CRISPR/Cas9. Curr. Protoc. Mol. Biol 128, e100. [PubMed: 31503414]
49. Sagné C, Isambert MF, Henry JP, and Gasnier B (1996). SDS-resistant aggregation of membrane proteins: application to the purification of the vesicular monoamine transporter. Biochem. J 316, 825–831. [PubMed: 8670158]

50. Mauthe M, Orhon I, Rocchi C, Zhou X, Luhr M, Hijlkema KJ, Coppes RP, Engedal N, Mari M, and Reggiori F (2018). Chloroquine inhibits autophagic flux by decreasing autophagosome-lysosome fusion. Autophagy 14, 1435–1455. [PubMed: 29940786]
51. Mauthe M, Jacob A, Freiberger S, Hentschel K, Stierhof YD, Codogno P, and Proikas-Cezanne T (2011). Resveratrol-mediated autophagy requires WIPI-1-regulated LC3 lipidation in the absence of induced phagophore formation. Autophagy 7, 1448–1461. [PubMed: 22082875]
52. Wu X, Wu FH, Wang X, Wang L, Siedow JN, Zhang W, and Pei ZM (2014). Molecular evolutionary and structural analysis of the cytosolic DNA sensor cGAS and STING. Nucleic Acids Res. 42, 8243–8257. [PubMed: 24981511]
53. Margolis SR, Wilson SC, and Vance RE (2017). Evolutionary Origins of cGAS-STING Signaling. Trends Immunol. 38, 733–743. [PubMed: 28416447]
54. Gillingham AK, Pfeifer AC, and Munro S (2002). CASP, the alternatively spliced product of the gene encoding the CCAAT-displacement protein transcription factor, is a Golgi membrane protein related to giantin. Mol. Biol. Cell 13, 3761–3774. [PubMed: 12429822]
55. Yao P, Potdar AA, Arif A, Ray PS, Mukhopadhyay R, Willard B, Xu Y, Yan J, Saidel GM, and Fox PL (2012). Coding region polyadenylation generates a truncated tRNA synthetase that counters translation repression. Cell 149, 88–100. [PubMed: 22386318]
56. Nazim M, Masuda A, Rahman MA, Nasrin F, Takeda JI, Ohe K, Ohkawara B, Ito M, and Ohno K (2017). Competitive regulation of alternative splicing and alternative polyadenylation by hnRNP H and CstF64 determines acetylcholinesterase isoforms. Nucleic Acids Res. 45, 1455–1468. [PubMed: 28180311]
57. Crow YJ, and Manel N (2015). Aicardi-Goutières syndrome and the type I interferonopathies. Nat. Rev. Immunol 15, 429–440. [PubMed: 26052098]
58. Liu Y, Jesus AA, Marrero B, Yang D, Ramsey SE, Sanchez GAM, Tenbrock K, Wittkowski H, Jones OY, Kuehn HS, et al. (2014). Activated STING in a vascular and pulmonary syndrome. N. Engl. J. Med 371, 507–518. [PubMed: 25029335]
59. Dooley HC, Razi M, Polson HEJ, Girardin SE, Wilson MI, and Tooze SA (2014). WIPI2 links LC3 conjugation with PI3P, autophagosome formation, and pathogen clearance by recruiting Atg12-5-16L1. Mol. Cell 55, 238–252. [PubMed: 24954904]
60. Strong LM, Chang C, Riley JF, Boecker CA, Flower TG, Buffalo CZ, Ren X, Stavoe AK, Holzbaur EL, and Hurley JH (2021). Structural basis for membrane recruitment of ATG16L1 by WIPI2 in autophagy. Elife 10, e70372. [PubMed: 34505572]
61. Li D, and Roberts R (2001). WD-repeat proteins: structure characteristics, biological function, and their involvement in human diseases. Cell. Mol. Life Sci 58, 2085–2097. [PubMed: 11814058]
62. Konno H, Konno K, and Barber GN (2013). Cyclic dinucleotides trigger ULK1 (ATG1) phosphorylation of STING to prevent sustained innate immune signaling. Cell 155, 688–698. [PubMed: 24119841]
63. Wilton J, de Mendonça FL, Pereira-Castro I, Tellier M, Nojima T, Costa AM, Freitas J, Murphy S, Oliveira MJ, Proudfoot NJ, and Moreira A (2023). Pro-inflammatory polarization and colorectal cancer modulate alternative and intronic polyadenylation in primary human macrophages. Preprint at bioRxiv. 10.1101/2023.02.24.529734.
64. Germic N, Frangez Z, Yousefi S, and Simon HU (2019). Regulation of the innate immune system by autophagy: monocytes, macrophages, dendritic cells and antigen presentation. Cell Death Differ. 26, 715–727. [PubMed: 30737475]
65. Wen JH, Li DY, Liang S, Yang C, Tang JX, and Liu HF (2022). Macrophage autophagy in macrophage polarization, chronic inflammation and organ fibrosis. Front. Immunol 13, 946832. [PubMed: 36275654]
66. Ohkuri T, Kosaka A, Ishibashi K, Kumai T, Hirata Y, Ohara K, Nagato T, Oikawa K, Aoki N, Harabuchi Y, et al. (2017). Intratumoral administration of cGAMP transiently accumulates potent macrophages for anti-tumor immunity at a mouse tumor site. Cancer Immunol. Immunother 66, 705–716. [PubMed: 28243692]
67. Yamazaki T, Liu L, Conlon EG, and Manley JL (2020). Burkitt lymphoma-related TCF3 mutations alter TCF3 alternative splicing by disrupting hnRNPH1 binding. RNA Biol. 17, 1383–1390. [PubMed: 32449435]

68. Thomson JA, Itskovitz-Eldor J, Shapiro SS, Waknitz MA, Swiergiel JJ, Marshall VS, and Jones JM (1998). Embryonic stem cell lines derived from human blastocysts. Science 282, 1145–1147. [PubMed: 9804556]
69. Jiao S, Guan J, Chen M, Wang W, Li C, Wang Y, Cheng Y, and Zhou Z (2018). Targeting IRF3 as a YAP agonist therapy against gastric cancer. J. Exp. Med 215, 699–718. [PubMed: 29339449]
70. Schindelin J, Arganda-Carreras I, Frise E, Kaynig V, Longair M, Pietzsch T, Preibisch S, Rueden C, Saalfeld S, Schmid B, et al. (2012). Fiji: an open-source platform for biological-image analysis. Nat. Methods 9, 676–682. [PubMed: 22743772]
71. Martin M (2011). Cutadapt removes adapter sequences from highthroughput sequencing reads. EMBnet. J 17, 10–12.
72. Bray NL, Pimentel H, Melsted P, and Pachter L (2016). Near-optimal probabilistic RNA-seq quantification. Nat. Biotechnol 34, 525–527. [PubMed: 27043002]
73. Pimentel H, Bray NL, Puente S, Melsted P, and Pachter L (2017). Differential analysis of RNA-seq incorporating quantification uncertainty. Nat. Methods 14, 687–690. [PubMed: 28581496]
74. Frankish A, Diekhans M, Jungreis I, Lagarde J, Loveland JE, Mudge JM, Sisu C, Wright JC, Armstrong J, Barnes I, et al. (2021). GENCODE 2021. Nucleic Acids Res. 49, D916–D923. [PubMed: 33270111]
75. Okita K, Matsumura Y, Sato Y, Okada A, Morizane A, Okamoto S, Hong H, Nakagawa M, Tanabe K, Tezuka K.i., et al. (2011). A more efficient method to generate integration-free human iPS cells. Nat. Methods 8, 409–412. [PubMed: 21460823]
76. Patel S, and Jin L (2019). TMEM173 variants and potential importance to human biology and disease. Genes Immun. 20, 82–89. [PubMed: 29728611]
77. Oslowski CM, and Urano F (2011). Measuring ER stress and the unfolded protein response using mammalian tissue culture system. Methods Enzymol. 490, 71–92. [PubMed: 21266244]
78. Woodward JJ, Iavarone AT, and Portnoy DA (2010). c-di-AMP secreted by intracellular Listeria monocytogenes activates a host type I interferon response. Science 328, 1703–1705. [PubMed: 20508090]
79. Vossaert L, O'Leary T, Van Neste C, Heindryckx B, Vandesompele J, De Sutter P, and Deforce D (2013). Reference loci for RT-qPCR analysis of differentiating human embryonic stem cells. BMC Mol. Biol 14, 21. [PubMed: 24028740]
80. Radonic A, Thulke S, Bae HG, Müller MA, Siegert W, and Nitsche A (2005). Reference gene selection for quantitative real-time PCR analysis in virus infected cells: SARS corona virus, Yellow fever virus, Human Herpesvirus-6, Camelpox virus and Cytomegalovirus infections. Virol. J 2, 7. [PubMed: 15705200]
81. Scotto-Lavino E, Du G, and Frohman MA (2006). 3' end cDNA amplification using classic RACE. Nat. Protoc 1, 2742–2745. [PubMed: 17406530]
82. Wittig I, Braun HP, and Schaägger H (2006). Blue native PAGE. Nat. Protoc 1, 418–428. [PubMed: 17406264]
83. Klionsky DJ, Abdel-Aziz AK, Abdelfatah S, Abdellatif M, Abdoli A, Abel S, Abeliovich H, Abildgaard MH, Abudu YP, Acevedo-Arozena A, et al. (2021). Guidelines for the use and interpretation of assays for monitoring autophagy (4th edition). Autophagy 17, 1–382. [PubMed: 33634751]

Highlights

- Alternative polyadenylation of WDR33 transcripts produces 3 isoforms: V1, V2, and V3
- V1 is a nuclear poly(A) factor, but V2 and V3 are ER proteins that regulate STING
- V2 interacts with STING and represses IFNB1 by preventing STING oligomerization
- V2 also interacts with WIPI2 isoforms to promote STINGinduced autophagy

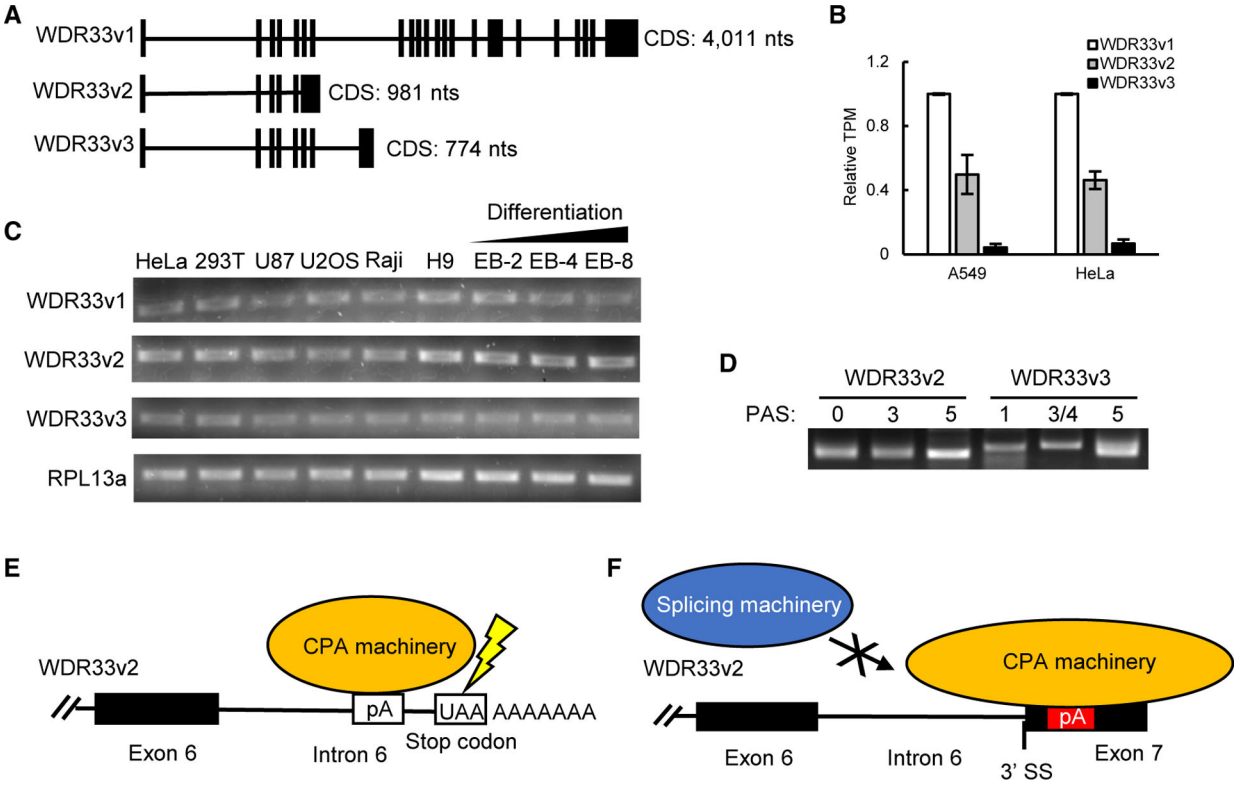

Figure 1. WDR33 isoform mRNAs are generated by APA

(A) Schematics of WDR33 mRNA variants (not drawn to scale).

(B) Relative mRNA abundances (transcripts per million [TPM]) of WDR33 isoform mRNAs normalized to V1 based on HeLa and A549 RNA-seq data. Data are shown as means ± standard deviation (SD) from three replicates.

(C) WDR33 isoform mRNA expression measured by RT-PCR in the indicated cell lines. EB, embryoid body. See also Figure S1A.

(D) Functional V2 and V3 PASs detected by 3′ RACE using HeLa RNA. See also Figures S1B and S1C.

(E and F) Schematics showing how V2 PAS0 usage generates a 3′ UTR-lacking mRNA (E) and how V2 PAS3 usage causes intron 6 retention by interfering with splicing (F). pA, polyadenylation site.

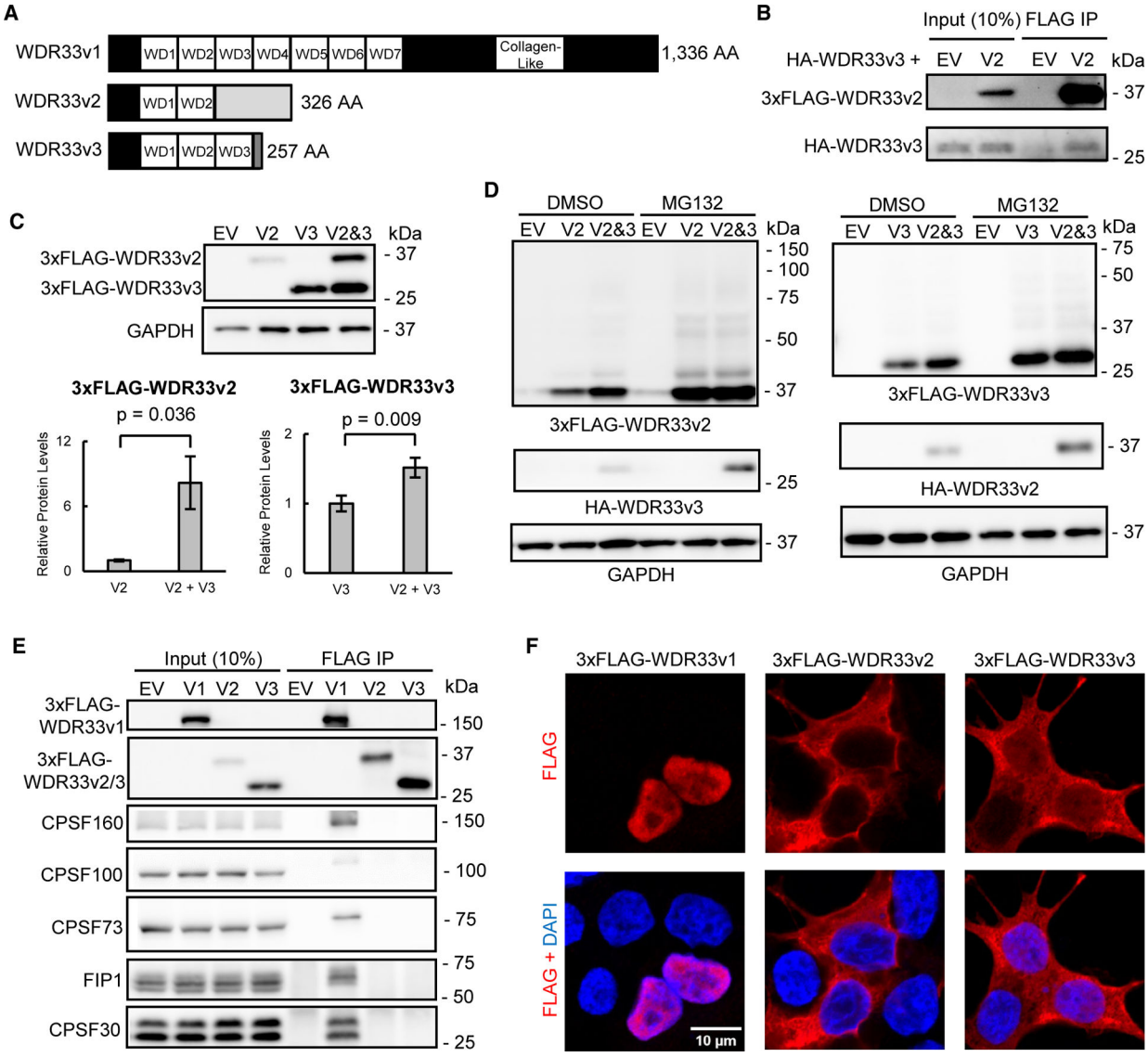

Figure 2. V2 and V3 are not polyadenylation factors

(A) Schematics of WDR33 protein isoforms (not drawn to scale). AA, amino acid.

(B) Co-immunoprecipitation (coIP) western blot (WB) of co-transfected 33FLAG-V2 and HA-V3 in 293T cells. EV, empty vector.

(C) Protein levels of co-transfected 3×FLAG-V2 and V3 measured by WB (top) in 293T cells and quantifications (means ± SD from three replicates) of 3×FLAG-V2 (bottom left) and V3 (bottom right). Student's t test was performed, with $p < 0.05$ considered significant. See also Figure S2C.

(D) Protein levels of 3×FLAG-V2 (left) and V3 (right) measured by WB with or without HA-V3 or V2 co-expression, respectively, after DMSO or MG132 treatment in 293T cells.

(E) CoIP WB of 33FLAG-EV/V1/V2/V3 with the indicated CPSF subunits in 293T cells. See also Figure S2D.

(F) Localization of WDR33 isoforms determined by immunofluorescence in 293T cells. Scale bar, 10 μm. See also Figure S2H.

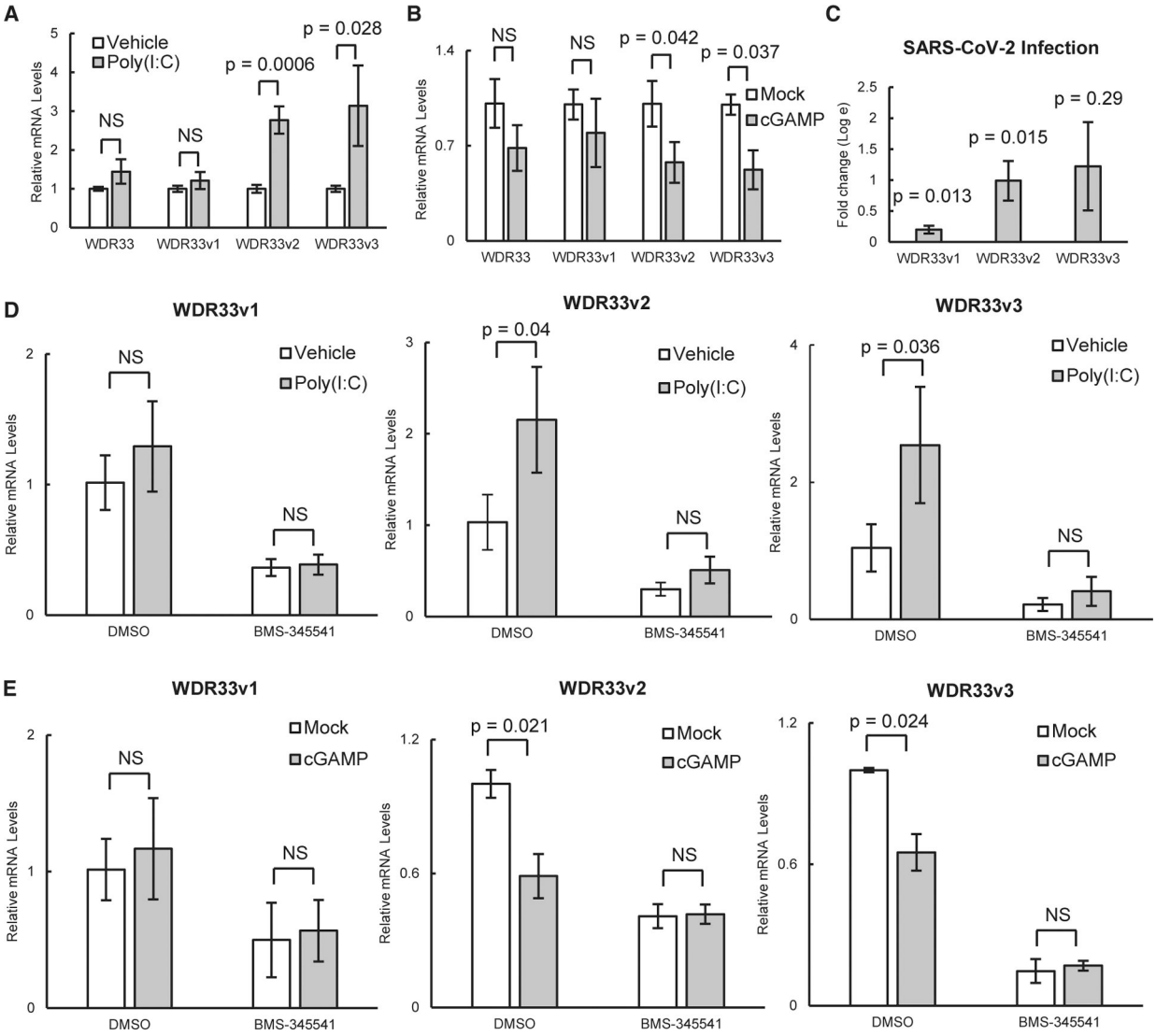

Figure 3. V2 and V3 are involved in immune responses and are regulated by the NF-κB pathway

(A and B) mRNA expression of total WDR33, V1, V2, and V3 measured by RT-qPCR in HeLa cells treated with vehicle or poly(I:C) (A; see also Figure S3A) and in BJ cells treated with mock or cGAMP at 50 μM for 6 h (B; see also Figure S3B).

(C) Fold changes (logarithmic scale) of V1, V2, and V3 mRNAs by RNA-seq analysis of ACE2-transfected A549 cells after SARS-CoV-2 infection. See also Table S1.

(D and E) mRNA expression of V1 (left), V2 (middle), and V3 (right) measured by RT-qPCR in HeLa cells treated with DMSO or BMS-345541 with or without poly(I:C) (D; see also Figure S3E) and in BJ cells treated with DMSO or BMS-345541 with or without cGAMP (E; see also Figure S3F).

All bar graphs are shown as means ± SD from three replicates except for (C), where data are shown as log e fold changes ± standard error from three replicates. Student's t tests were performed except for (C). For (C), Wald test was performed, and the reported p values were adjusted for false discovery rate. $p < 0.05$ was considered significant. NS, not significant.

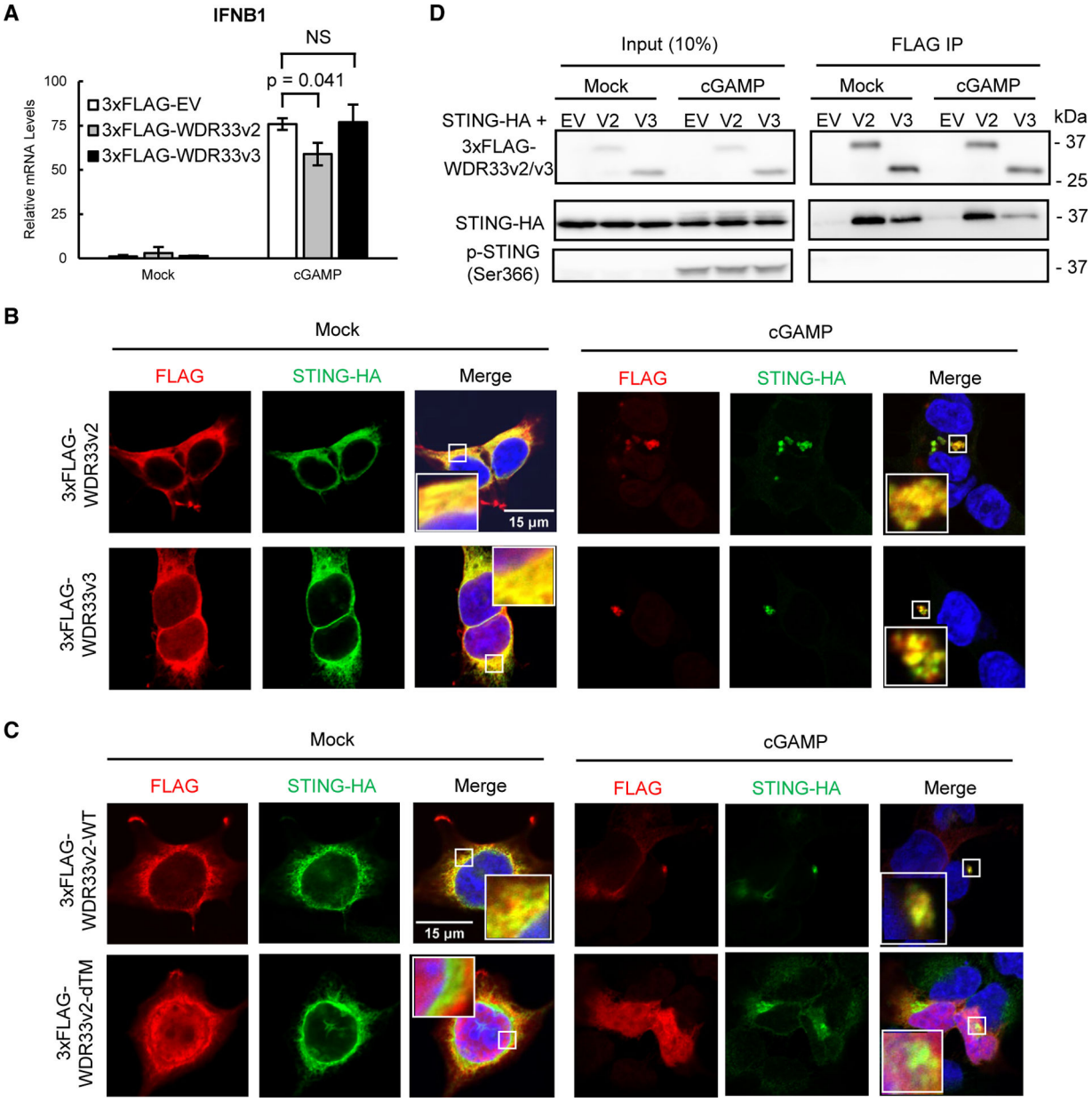

Figure 4. V2 and V3 are functionally related to STING

(A) IFNB1 mRNA expression measured by RT-qPCR in EV/V2/V3-transfected BJ cells with or without cGAMP at 50 μM for 6 h. Data are shown as means ± SD from three replicates. EV, empty vector. Student's t tests were performed, with $p < 0.05$ considered significant. NS, not significant. See also Figures S3I–S3K.

(B and C) Co-localization of transfected 33FLAG-V2/V3 (B) or 33FLAG-V2-dTM (C) with STING-HA with or without cGAMP at 100 μM for 30 min determined by immunofluorescence in 293T cells. Scale bars, 15 μm. See also Figures S4A and S4B.

(D) CoIP WB of 33FLAG-EV/V2/V3 with STING-HA and Ser366-phosphorylated STING with or without cGAMP in 293T cells. See also Figure S4C.

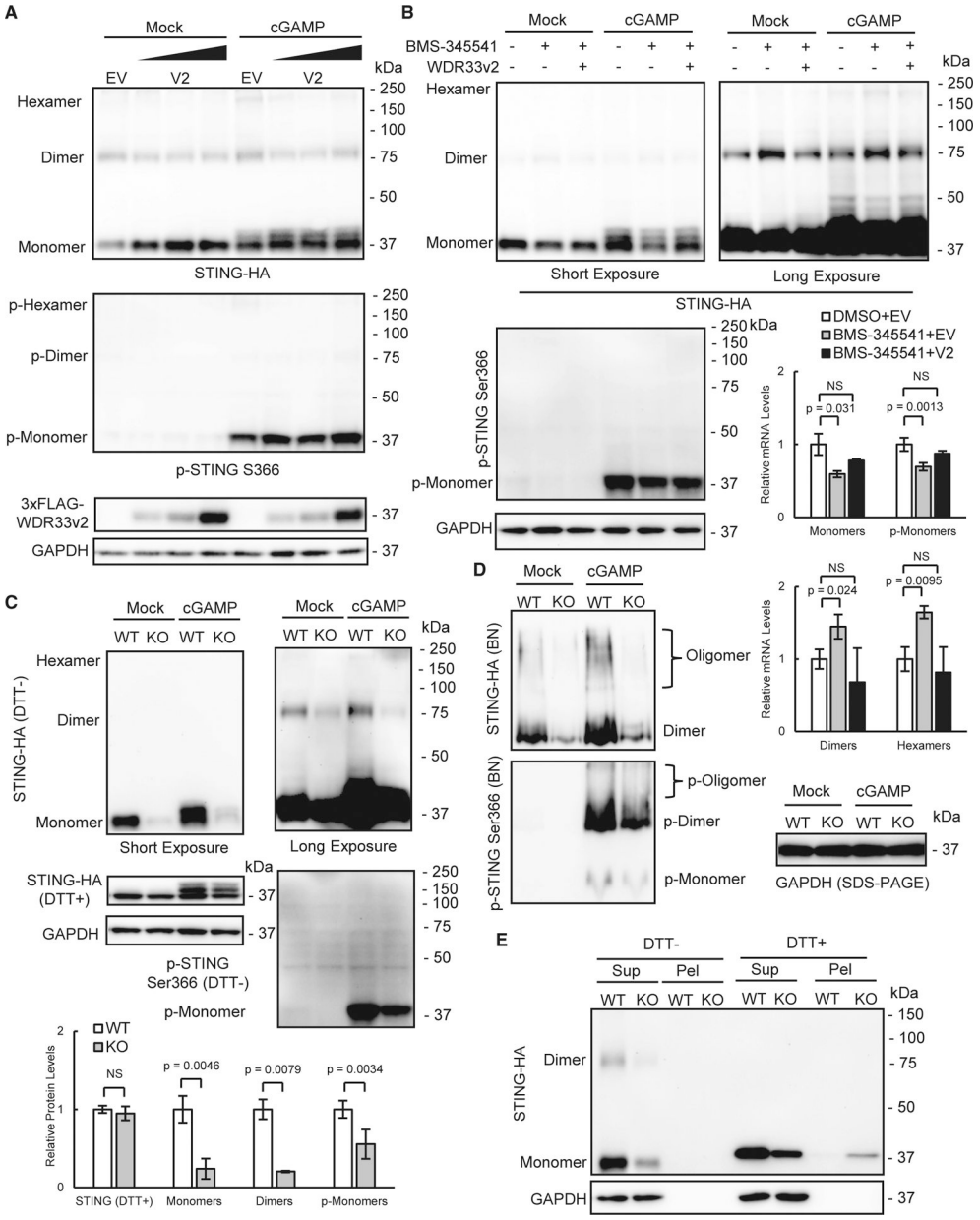

Figure 5. V2 decreases STING disulfide oligomer accumulation and increases p-STING monomer accumulation

(A) STING oligomerization detected by non-reducing WB of STING-HA and p-STING (Ser366) in 293T cells transfected with empty vector (EV) or 3×FLAG-V2 with or without cGAMP. See also Figure S5A.

(B) STING oligomerization with or without cGAMP detected by non-reducing WB (top) of STING-HA and p-STING (Ser366) in 293T cells treated with DMSO or BMS-345541, with or without V2 rescue, and quantification (bottom right) of levels of STING monomers, dimers, hexamers, and p-STING monomers under cGAMP stimulation. See also Figure S5E.

(C) STING oligomerization detected by non-reducing WB (top) of STING-HA and p-STING (Ser366) in WT and V2-KO 293T cells with or without cGAMP, and quantification

(bottom) of levels of STING monomers, dimers, and p-STING monomers (with cGAMP) and levels of total STING (with DTT, without cGAMP). See also Figures S5F and S5G.
(D) STING oligomerization detected by BN gel of STING-HA and p-STING (Ser366) in WT and V2-KO 293T cells with or without cGAMP.
(E) STING protein levels from WT and V2-KO cells detected by WB in the Triton/NP-40 soluble (Sup) or insoluble (Pel) fractions with or without DTT.
All bar graphs are shown as means ± SD from three replicates. Student's t tests were performed, with $p < 0.05$ considered significant. NS, not significant.

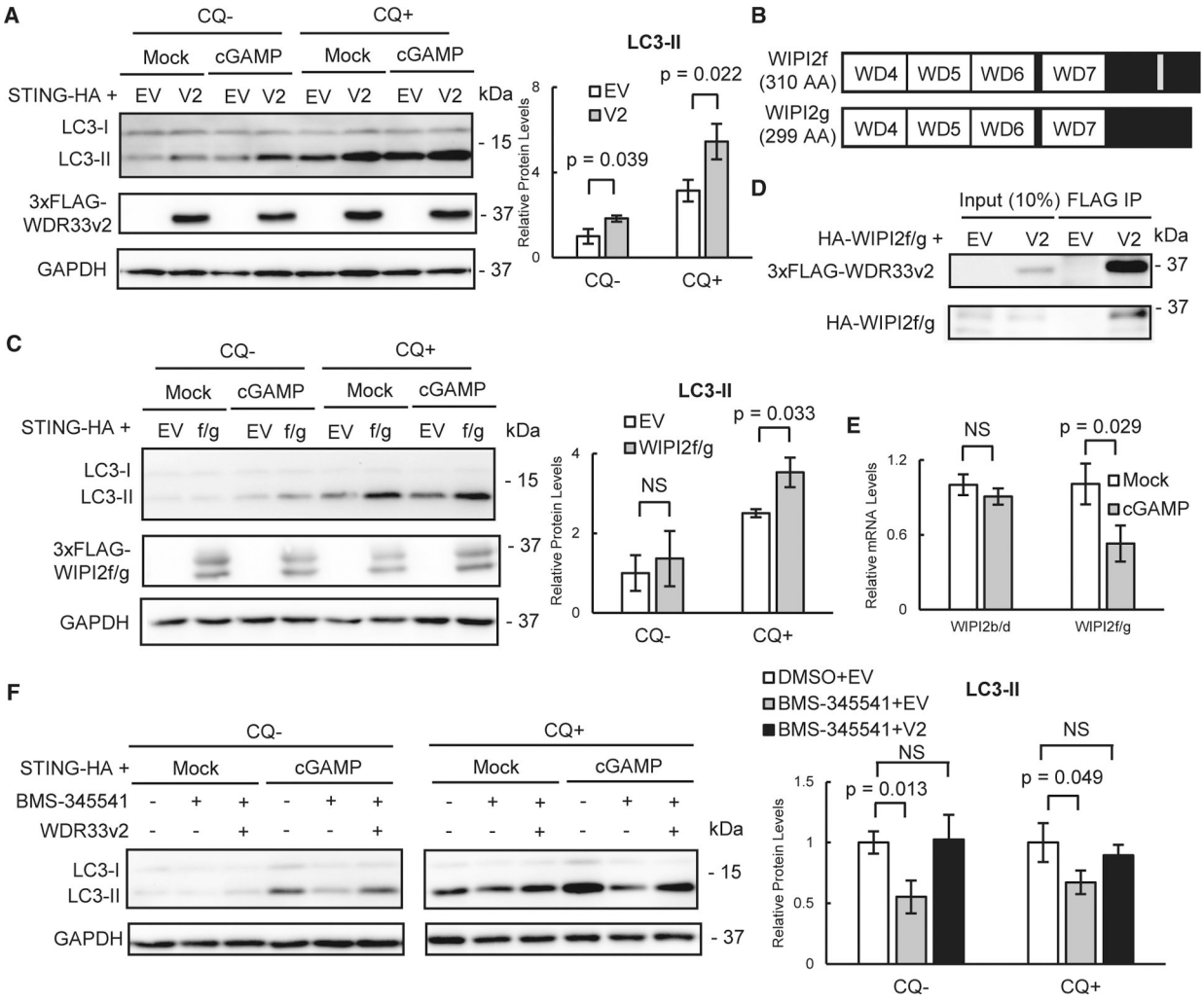

Figure 6. V2 facilitates STING-mediated autophagy

(A) Protein levels of LC3-I and LC3-II measured by WB (left) in 293T cells transfected with empty vector (EV) or 33FLAG-V2 with or without cGAMP or CQ, and quantification (right) of LC3-II (with cGAMP).

(B) Schematics of WIPI2f/g protein domains (not drawn to scale). See also Figure S6B.

(C) Protein levels of LC3-I and LC3-II measured by WB (left) in 293T cells transfected with EV or 33FLAG-WIPI2f/g (f/g) with or without cGAMP or CQ, and quantification (right) of LC3-II (with cGAMP).

(D) CoIP WB of co-transfected 33FLAG-V2 and HA-WIPI2f/g (f/g) in 293T cells. See also Figure S6D.

(E) mRNA expression of WIPI2b/d and WIPI2f/g measured by RT-qPCR in BJ cells treated with mock or cGAMP at 50 μM for 6 h.

(F) Protein levels of LC3-I and LC3-II with or without cGAMP or CQ measured by WB (left) in 293T cells treated with DMSO or BMS-345541, with or without V2 rescue, and quantification (right) of LC3-II (with cGAMP).

All bar graphs are shown as means ± SD from three replicates. Student's t tests were performed, with $p < 0.05$ considered significant. NS, not significant.

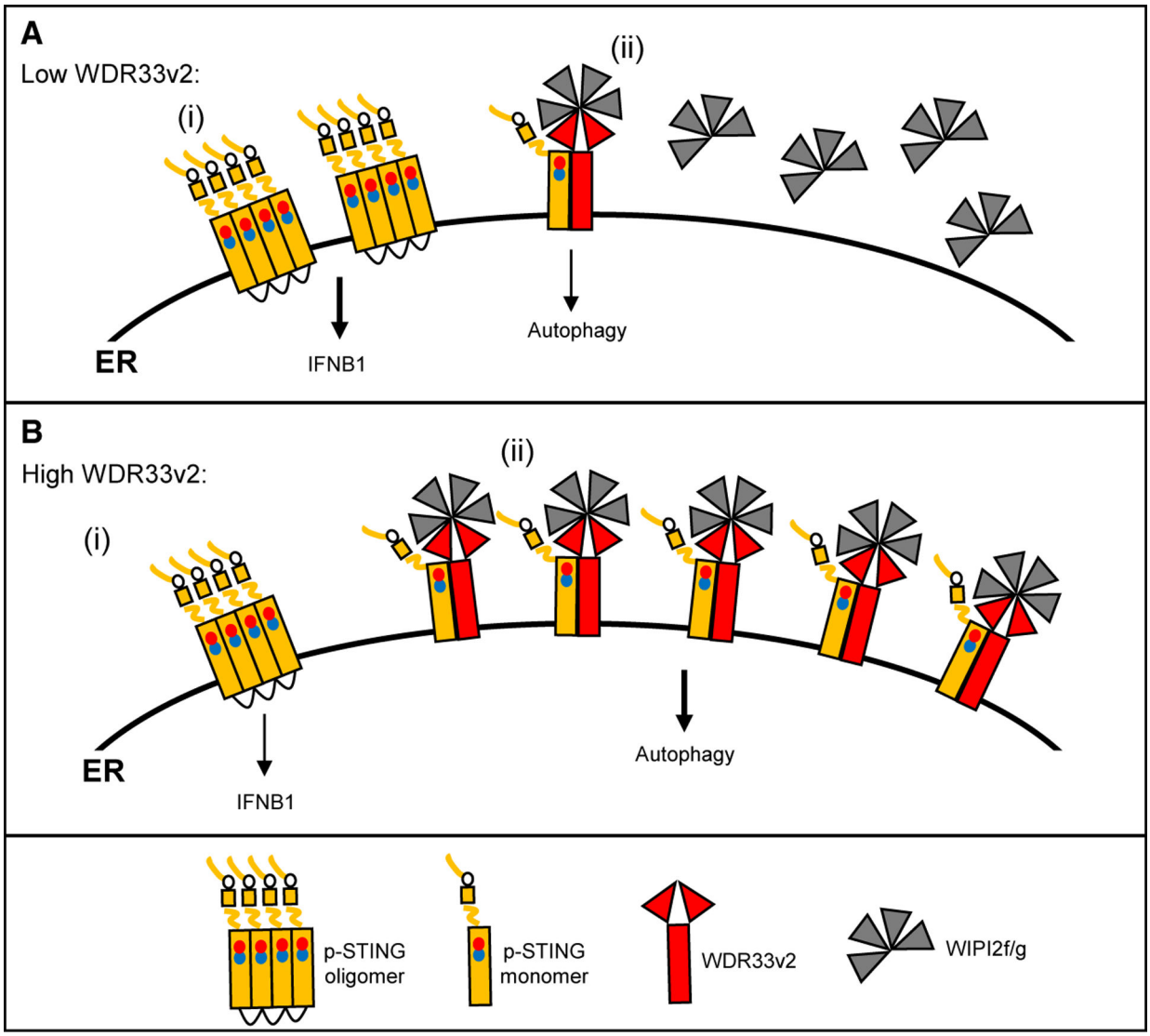

Figure 7. Model of V2 in STING-mediated innate immune responses

(A) When V2 expression is low, STING freely forms disulfide oligomers to induce IFNB1 upon cGAMP activation (i). Some STING monomers interact with V2/WIPI2f/g to induce autophagy (ii).

(B) When V2 expression is high, there is less STING disulfide oligomers to induce IFNB1 (i), but more STING monomers to interact with V2/WIPI2f/ g to induce stronger autophagic activity (ii).

KEY RESOURCES TABLE

REAGENT or RESOURCE	SOURCE	IDENTIFIER
Antibodies		
Mouse anti-FLAG	Sigma-Aldrich	Cat# F1804; RRID: AB_262044
Mouse anti-HA	Biolegend	Cat# 901533; RRID: AB_2801249
Goat anti-HA	Bethyl Laboratories	Cat# A190-138A; RRID: AB_2631894
Rabbit anti-GAPDH	Sigma-Aldrich	Cat# G9545; RRID: AB_796208
Mouse anti-CPSF1	Santa Cruz Biotechnology	Cat# sc-166281; RRID: AB_2084362
Rabbit anti-CPSF1	Abclonal	Cat# A17144; RRID: AB_2769032
Mouse anti-CPSF2	Santa Cruz Biotechnology	Cat# sc-165983; RRID: AB_2084371
Mouse anti-CPSF3	Santa Cruz Biotechnology	Cat# sc-393001
Rabbit anti-CPSF73	Abclonal	Cat# A2222
Rabbit anti-FIP1L1	Abclonal	Cat# A7138; RRID: AB_2767693
Rabbit anti-CPSF30	Bethyl Laboratories	Cat# A301-584A; RRID: AB_1078872
Rabbit anti-TMEM173/STING	Proteintech	Cat# 19851-1-AP; RRID: AB_10665370
Rabbit anti-phospho-STING (Ser366)	Cell Signaling Technology	Cat# 19781S; RRID: AB_2737062
Rabbit anti-TBK1	Proteintech	Cat# 28397-1-AP; RRID: AB_2881132
Rabbit anti-phospho-TBK1 (Ser172)	Proteintech	Cat# 82383-1-RR; RRID: AB_3076688
Rabbit anti-LC3B	Cell Signaling Technology	Cat# 2775S; RRID: AB_915950
Bacterial and virus strains		
DH5α	Invitrogen	Cat# 18265017
Stbl2	Invitrogen	Cat# 10268019
Biological samples		
Raji cell total RNA	Yamazaki et al.[67]	N/A
Chemicals, peptides, and recombinant proteins		
Poly(I:C)	Tocris	Cat# 4287
2′3′-cGAMP	Invivogen	Cat# tlrl-nacga23
Interferon-β	Bio-Techne	Cat# 8499-IF
MG132	MedChemExpress	Cat# HY-13259
BMS-345541	Adooq Bioscience	Cat# A11318
Chloroquine	Sigma-Aldrich	Cat# C6629
Deposited data		
293 Ribosome profiling	Clamer et al.[31]	GSE112353
HeLa RNA-seq	Kamieniarz-Gdula et al.[29]	GSE123105
A549 SARS-CoV-2-infection RNA-seq	Blanco-Melo et al.[30]	GSE147507
Experimental models: Cell lines		
HeLa	ATCC	CCL-2
HEK293T	ATCC	CRL-3216
U-2 OS	ATCC	HTB-96
U-87 MG	ATCC	HTB-14
WA09 (H9 human embryonic stem cells)	Thomson et al.[68]	NIHhESC-10-0062

REAGENT or RESOURCE	SOURCE	IDENTIFIER
cGAS$^{-/-}$ BJ-5ta	Bodnar et al.[38] Ng et al.[39]	N/A
WDR33v2$^{dTM/dTM}$ HEK293T	This paper	N/A
Oligonucleotides		
MISSION® siRNA Universal Negative Control #1	Sigma-Aldrich	Cat# SIC001
siIRF3 5′ UAUCAGAAGUACUGCCUCC 3′ (anti-sense)	Jiao et al.[69]	N/A
Human WDR33 Intron 6 5′ gRNA 5′ TTCTGTAGTCCCTATTGTCA 3′	This paper	N/A
Human WDR33 Intron 6 3′ gRNA 5′ TGAATGTCGTCAGCTAACAT 3′	This paper	N/A
RT-PCR primers	This paper	Table S2
Recombinant DNA		
pcDNA3-3×FLAG-WDR33v1	This paper	N/A
pcDNA3-3×FLAG-WDR33v2	This paper	N/A
pcDNA3-3×FLAG-WDR33v3	This paper	N/A
pcDNA3-HA-WDR33v2	This paper	N/A
pcDNA3-HA-WDR33v3	This paper	N/A
pcDNA3-STING-HA	This paper	N/A
pcDNA3-3×FLAG-CANX	This paper	N/A
pcDNA3-EMD-3×FLAG	This paper	N/A
pCXS-3×FLAG-EV	This paper	N/A
pCXS-3×FLAG-WDR33v2	This paper	N/A
pCXS-3×FLAG-WDR33v3	This paper	N/A
pCXS-3×FLAG-WIPI2bd	This paper	N/A
pCXS-3×FLAG-WIPI2fg	This paper	N/A
PX458	Ran et al.[47]	Addgene# 48138
PX459 V2.0	Ran et al.[47]	Addgene# 62988
Software and algorithms		
FIJI ImageJ	Schindelin et al.[70]	https://imagej.net/software/fiji/
TMHMM 2.0	Krogh et al.[33]	https://services.healthtech.dtu.dk/services/TMHMM-2.0/
TMPred	Hofmann and Stoffel[34]	http://embnet.vital-it.ch/software/TMPRED_form.html
Cutadapt	Martin[71]	https://cutadapt.readthedocs.io/en/stable/
kallisto	Bray et al.[72]	https://pachterlab.github.io/kallisto/
Sleuth	Pimentel et al.[73]	https://pachterlab.github.io/sleuth/
GENCODE human transcriptome (GRCh38.p13)	Frankish et al.[74]	https://www.gencodegenes.org/